MeV Kr ION INDUCED MIXING IN Si-Ge MULTILAYERS

A Thesis Submitted
in Partial Fulfilment of the Requirements
for the Degree of
MASTER OF TECHNOLOGY

by
BISHAKHA BHATTACHARYA

to the
MATERIALS SCIENCE PROGRAMME
INDIAN INSTITUTE OF TECHNOLOGY, KANPUR
JULY, 1995

MSP-1995-M-BHA-MeV

CERTIFICATE

It is certified that the work contained in the thesis entitled "MeV Kr ION INDUCED MIXING IN Si-Ge MULTILAYERS" by BISHAKHA BHATTACHARYA has been carried out under our supervision and this work has not been submitted elsewhere for a degree.

Dr. Y. N. Mohapatra
Materials Science Programme,
I.I.T. Kanpur.

July 1995

Dr. V.N. Kulkarni
Department of Physics,
I.I.T. Kanpur.

July 1995

ACKNOWLEDGEMENT

I take this oppurtunity to express my indebtedness to my supervisors Dr. Y.N. Mohapatra and Dr.V.N. Kulkarni for their valuable guidance throughout my M.Tech programme. I am specially grateful to them for their seemingly endless patience with me and my work during my troubled times.

I would also like to thank my lab mates, Sankar (da) Dhar for teaching me the involved experimental techniques and helping me out with his experience in all my experiments and Tapo(da)brata for keeping us in high spirits and giving his time as and when required, my seniors Ram(ki)akrishnan and Paritosh (da) for their ground work in Si/Ge system for their thesis and hence their advice. I am grateful to Anil Sinha who had to devote a considerable part of his valuable time to help me characterize my samples. Support from the staff of the Central Nuclear Laboratory and the Physics Workshop has been very vital. The presence of Pravat Giri(da), Sandeep, Debasish(da), Bidyut(da) and Roy is also acknowledged.

Without the care and advise of Dr.A.K. Dutta, Dr.(Mrs.) Borwankar, Dr. S. Razdan I might not have been able to complete the programme even now. Needless to say, my family members and friends have helped me at every step towards the completion of my thesis and otherwise.

A B S T R A C T

The Si-Ge system is important due to its potential application in optoelectronic and photonic technology. Ion beam mixing can provide a powerful method for synthesizing Si-Ge alloy of desired composition on a preselected region of the sample at considerably lower temperatures as compared to the conventional methods. The efficacy of the ion beam mixing of this system was not evaluated in detail. Bearing in mind the advantages of multilayers in the synthesis of alloys of variable/predetermined composition, Si and Ge films were deposited alternately on a quartz substrate using an electron gun to evaporate the elements in high vacuum. TRIM calculations were carried out to determine the range and energy deposition, distribution of 1 MeV Kr ions in Si-Ge. The total multilayer thickness of the samples was selected from these calculations such that most of the ions pass through the multilayer,yet deposit a significant part of their energy in it. The number of films varied between 6-10 layers. The thickness of the individual films were between 250 to 350 A^{O}.

Ion mixing experiments were performed using Krypton ions of energy 1.0 MeV. The irradiation dose was varied between $8 \times 10^{15}$to 5×10^{16} at/cm^2. The irradiation was carried out for different temperatures up to 300^{o}C. The samples were characterized using RBS, XRD, Transmission Spectroscopy and four probe measurements.

Detailed simulation analysis of the RBS spectra was carried out to extract information about the mixing and the variation in composition as a result of irradiation.

The RBS analysis shows that there is definitely a mixing at room temperature which is expected from the TRIM calculations. Mixing has occurred at all the interfaces for high doses at room temperature. The mixing observed enhances significantly with the increase in temperature with the thickness of the mixed region showing a steep rise from room temperature to 200^{o}C. However a further increase in temperature to 250^{o}C shows no significant change in mixing. Moreover, at a temperature of 300^{o}C the mixing reduces and appears almost equivalent to room temperature mixing. The increase in mixing at 200^{o}C is because of Radiation Enhanced Diffusion as the critical temperature of the system is around 200^{o}C. The fall in mixing at 300^{o}C could be because of strain relaxation and highly disordered nature of the mixed layer. Investigation into such retarding mechanism is required.

The optical characterization was undertaken to find the band gap of the material. However, as the films are amorphous in nature even after annealing, the band gap obtained was ~ 0.8 eV for all the samples irrespective of irradiating conditions. This is because of tail end mixing in the amorphous semiconductors.

A low temperature heat treatment (620^{o}C for 15 minutes in flowing dry nitrogen) is enough to improve the conductivity indicating the removal of ion induced damages. The increase in resistivity with dose implies that the damage has not been fully recovered. The decrease in resistivity with rise in substrate temperature during irradiation shows the possibility of in situ annealing of the defects produced during ion irradiation.

CONTENTS

Chapter 1 : Introduction

1.1 Surface Modification by Ion Processes.....1
1.2 Sample configurations in IBM.....3
1.3 Demonstrated applications of Ion Beam Mixing..... 4
1.4 Mechanism of Mixing.....5
1.5 Ion Beams in Semiconductors and the Si-Ge Alloy System.....7

Chapter 2 : Experimental Details

General.....11
2.1 Sample Design.....11
2.2 Transport and range of ions in matter.....12
2.3 Sample preparation.....14
2.4 Heavy Ion Irradiation.....15
2.5 Annealing.....16
2.6 Ion Beam Analysis.....17
2.7 RBS and RUMP simulation package.....18
2.8 Optical Characterization.....19
2.9 Resistivity Measurements.....20

Chapter 3 : Results and Discussions

General.....22
3.1 RBS measurements and results.....22
3.1.1 Typical RBS spectrum of a multilayered sample.....22
3.1.2 Configuration 1: six alternate Si and Ge layers on quartz.....24
3.1. Configuration 11: ten alternate Si and Ge layers on quartz..... 29
3.2 Mixing Mechanism.....36
3.3 Transmission Spectroscopy.....41
3.4 Resistivity Measurements..... 42

Chapter 4 : Summary and Conclusions.....45

Figures
References

LIST OF FIGURES

Fig. 2.1 Multi layer and the effect of ion beam irradiation 48

Fig. 2.2(a) TRIM calculations to estimate the total thickness of the sample. The fig. shows the energy deposited by the incident ion in the target. 49

Fig. 2.2(b) TRIM calculations showing the range of Krypton ions in the substrate. 50

Fig. 2.3 The Heavy Ion Irradiation Chamber 51

Fig. 2.4 Experimental arrangement for annealing the samples 52

Fig. 2.5 The RBS Chamber 53

Fig.2.6 Schematic diagram of a typical apparatus used in backscattering spectrometry 54

Fig. 2.7 Practical situation of a thin film on a transparent substrate for transmission spectroscopy 5

Fig. 2.8 Typical Transmission Spectra obtained from thin films 55

Fig. 2.9 Outlay of the apparatus used in the transmission spectroscopy 56

Fig. 2.11 The four point probe arrangement for resistivity measurements 56

Fig. 3.1 Typical RBS spectra obtained from multilayer sample. 57

Fig. 3.2 RBS spectra of the as evaporated sample along with the simulated curve (6 - layer) 58

Fig. 3.3 The 6 layerd sample configuration 25

Fig. 3.4 RBS spectra for the sample irradiated with a dose of 2×10^{16} at/cm^2 at room temperature with the simulated curve 59

g. 3.5 RBS spectra for the sample irradiated with a se of $3x10^{16}$ at/cm^2 at room temperature with the mulated curve 60

g. 3.6 RBS spectra for the sample irradiated with a se of $5x10^{16}$ at/cm^2 at room temperature with the mulated curve 61

g. 3.7 TRIM calculations for the 6 layered samples owing the energy deposited by the incident ion 62

g. 3.8 Plot showing the variation of the mixed hickness with dose for room temperature irradiation 63

ig. 3.9 Sample configuration for 10 layered sample 30

ig. 3.10 RBS spectra for the sample irradiated with a dose of $1x10^{16}$ at/cm^2 at room temperature 64

ig. 3.11 RBS spectra for the sample irradiated with a dose of $1x10^{16}$ at/cm^2 at 200^{o}C (High T) 65

ig. 3.12 RBS spectra for the sample irradiated with a dose of $1x10^{16}$ at/cm^2 at 250^{o}C (High T) 66

ig. 3.13 TRIM calculations for the 10 layered samples howing the energy deposited by the incident ion 67

ig .3.14 Comparison of the RBS spectra obtained from ample irradiated at 300^{o}with the as evaporated sample 68

Fig .3.15 Comparison of the RBS spectra obtained from sample irradiated at 300^{o}with the sample irradiated at room temperature 69

Fig. 3.16 Comparison of the RBS spectra to illustrate the progress in mixing with varying irradiating condition 70

Fig. 3.17 Comparison of the RBS spectra to illustrate the progress in mixing with varying irradiation condition 71

Fig. 3.18 Comparison of the RBS spectra to illustrate the progress in mixing with varying irradiation condition 72

Fig. 3.19(a) TRIM calculations showing the cascade formation along with the ion trajectory for Si/Ge bilayer with Ge on top 73

g. 3.19(b) TRIM calculations showing the cascade rmation along with the ion trajectory for Si/Ge bilayer th Ge on top 74

g. 3.20(a) TRIM calculations showing the cascade rmation along with the ion trajectory for Si/Ge bilayer th Si on top 75

g. 3.20(b) TRIM calculations showing the cascade rmation along with the ion trajectory for Si/Ge bilayer th Si on top 76

g. 3.21 Plot showing variation of the total mixed ickness with temperature 77

g. 3.22 Transmission spectra obtained during optical aracterization of the samples (for sample irradiated 200°C) 78

g. 3.23 Plot of α^2 vs ($h\nu$) 79

g. 3.24 Plot showing the variation of resistivity with se 80

g. 3.25 Plot showing the dependence room temperature sistivity on the substrate temperature during irradiation 81

LIST OF TABLES

Table 1.1 Comparison between ion beam mixing and ion implantation for the formation of alloys 3

Table 2.1 Estimated configuration of the sample for the formation of SiGe alloy 12

Table 3.1 Sample configuration of the 6 layered sample as revealed by RUMP simulations 24

Table 3.2 Configuration of the sample after irradiation with $2x10^{16}$ at/cm^2 at room temperature 27

Table 3.3 Configuration of the sample after irradiation with $3x10^{16}$ at/cm^2 at room temperature 28

Table 3.4 Configuration of the sample after irradiation with $5x10^{16}$ at/cm^2 at room temperature 28

Table 3.5 Sample configuration of the 10 layered sample as revealed by RUMP simulations 29

Table 3.6 Configuration of the sample after irradiation with $1x10^{16}$ at/cm^2 at room temperature 33

Table 3.7 Configuration of the sample after irradiation with $1x10^{16}$ at/cm^2 at 200° C 34

Table 3.8 Configuration of the sample after irradiation with $1x10^{16}$ at/cm^2 at 250° C 35

C H A P T E R 1

INTRODUCTION

1.1 Surface Modification by Ion Processes

Ion Implantation and Ion Beam Mixing provide unique ways to change the surface and near surface region of materials. The earliest use of an ion beam from a low energy accelerator to modify material properties was initiated in the early sixties in the form of doping of semiconductors by ion implantation instead of traditional thermal methods. It has now been adapted for modifying the properties of metals, ceramics and polymers. In the semiconductor industry it has been used to introduce a wide range of dopants with no masking complications, to produce buried layers, abrupt junctions, and precision alignment. Reproducibility from wafer to wafer, low processing temperatures and high degree of localization makes ion beams an important tool in the semiconductor industry.

Ion implantation is the introduction of one or more atomic species into the surface of the substrate material using energetic ion beams. This results in modified physical and chemical properties of the near surface region. The projectile incident on the target suffers a series of discrete collision events by which it slows down and transfers energy to the substrate [1].

Ion beam mixing, introduced in the early seventies, involves the use of ion beams to intermix or surface alloy a predeposited thin film with an underlying substrate or thin film [2].Ion beam mixing is being explored for the past several years as an alternative to direct

igh dose implantation [3].

An interesting aspect of ion implantation is that it roduces new solid phases. The possibility to produce equilibrium as ell as non-equilibrium (metastable) surface alloys without heating he material represents an important advantage of ion implantation. In ddition, high defect concentration produced in the collision cascades odifies considerably the diffusion coefficients and the thermodynamic limitations connected with the solid solubility can be surpassed and metastable alloys can be produced, in the form of either single phase solid solution or amorphous alloy. However, in terms of forming various alloy phases, the maximum obtainable composition by ion implantation is limited by the sputtering effect of the impinging ions as they loose their energy to the nuclei (atoms) in the near surface region of the material. Moreover, it would be even impossible to study various systems if the implanter available is not equipped with several versatile ion sources. In such cases ion beam mixing is suitable. In contrast to direct implantation, the ion beam used for ion beam mixing is typically an inert gas. It is used mainly to trigger atomic collisions for inducing intermixing between deposited material A and matrix B or A and B bilayer or multilayer on a substrate and thus forming an A-B alloy phase.

ble 1.1 Comparison between ion beam mixing and ion implantation for the formation of alloy phases [4].

Method	Effect of irradiation	Typical dose and obtainable alloy composition
Ion Mixing	Physical Mixing	10^{15} to 10^{16} ions/cm^2 No limitation on composition
Ion Implantation	Introducing alloy element	10^{17} to 10^{18} ions/cm^2 Sputtering effect limits the maximum composition to around 30%

1.2 Sample Configurations in IBM

Experimental investigation in the field of ion beam mixing have been executed with three main sample configurations :

(i) Bilayered samples where a thin film A is deposited on a substrate B

(ii) Thin marker samples in which an extremely thin layer (~1nm) of a marker element A is embedded in a matrix B

(iii) Multilayered samples in which the sample consists of a multiple sequence of very thin alternating films of two elements A and B on an inert substrate such as SiO_2.

Bilayer samples have been used primarily to investigate ion mixing of metal films on Si substrates. We have studied ion mixing in Si-Ge i.e. semiconductor-semiconductor system as well. The unique feature of bilayer configuration is that at early stages of ion irradiation, the supply of both materials A and B at the interface is constrained only by the process of ion mixing itself so that the

system is free to seek possible preferred compositions for the mixed region.

Very thin marker layer samples are used to investigate the basic aspects in ion mixing processes due to much simpler experimental conditions of a dilute impurity in an otherwise homogeneous host matrix.

Multilayered samples have been used primarily in metal-metal systems. Interest in this area has been spurred by the recognition that, through the use of ion mixing, metallic metastable, crystalline and amorphous phases can be formed quite readily. Multilayered structure is more convenient for producing alloys of desirable composition than bilayer because the composition is forced to a predetermined value which can be varied easily in a wide range by only adjusting the relative thickness of the individual layers. In these samples the average composition of the whole layer is fixed by the relative thickness of the respective layers of the constituents. For this reason these experiments are sometimes described as being performed in a limited supply configuration.

1.3 Demonstrated application of Ion Beam Mixing

Ion beam mixing is a technique for the modification of surface sensitive properties. The potential application of ion mixing depends on the different media that a solid surface can form an interface with ,eg. vacuum, plasma, gas, liquid, solid. For example the vacuum-solid interface can be altered by ion beam mixing to form a thin micro alloyed surface that has a lower vapor pressure than the bulk material, thus stabilizing it in vacuum. Optical properties and

work function can also be altered in a similar way of alloy formation, since these properties depend on the near surface parameter. In integrated circuit technology, the patterning of material could be envisaged by locally altering the surface to achieve selectivity in subsequent reactive ion etching processing. In case of solid-solid interface, changes in wear, friction, corrosion, adhesion etc. has been studied [6]. Other horizons for the application of ion beam mixing are the modification of electrical properties, the formation of metastable films of unique super conducting [7] and magnetic [8] properties.The potential benefits of surface ennoblement by ion beam mixing are so broad that the study of the properties of mixed layers is amply justified.

1.4 The Mechanism of Mixing

A great deal of effort has been expended in studying ion induced phase formation, including metastable and amorphous phases for various couples as a function of implantation temperature and ion fluence. Paine and Averback [9] reviewed the status of these ion beam mixing experiments of simple layered systems. These experiments have either utilized a bilayer or a thin marker layer in combination with Rutherford Backscattering (RBS) spectrometry to study the diffusion mechanism occurring during intermixing. The energy broadening of the RBS spectral peaks is a measure of the inter diffusion between the layers . The use of bilayer is most common as any binary composition can be attained during intermixing in this geometry.

During the initial impact period of implanted ions (less than 10^{-14}sec), molecular dynamic motion has been used [10] to

lescribe atomic motion. Different atomic transport mechanisms are)perative following ion penetration. For times within the first :x10^{-13} sec, collisional events prevail with atomic displacements well lescribed by two body collisions [11]. During this period only a :raction of events will be of high energy (KeV) recoil displacements vith the majority of displacements being in the multi-electronvolt regime. Hence substrate temperature is not important in this regime.

Following this displacement phase (up to 10^{-11} sec) the atomic motion is thermalized. Johnson et al. [12] have shown that for dense cascades in this time scale it is possible to predict, by thermodynamical considerations, which metallurgical phases can be expected to form and the criteria for the formation of amorphous phase during intermixing. For longer time periods (10^{-11} sec) atomic motion occurs by thermal diffusion of irradiation produced defects, ie. radiation enhanced diffusion. The depth scale associated with radiation enhanced diffusion is often several times the range of the initial ion.

Liu et al. postulated [13] a structural difference rule stating conditions for producing amorphous alloy films. These include

(i) The constituent layers have different structure

(ii) The composition after uniform mixing lies within the two phase region of the equilibrium phase diagram.

Therefore,in most situations, ion beam mixing can be attributed to one of several mechanisms :

(i) enhanced diffusion due to mobile defects such as vacancies and interstitials generated by the incoming ions.

(ii) Cascade mixing or repeated displacement of atoms in the

solid by successive collisions.

(iii) Mixing by energy spikes [56].

The mechanism of thermally assisted ion induced interface mixing evolves by the exchange of atoms at the interface of solids A and B resulting in a new inter atomic phase AB sandwiched between the elemental layers A and B[55]. The interface mixing now occurs between A and AB and/or between AB and B. The exchange of atoms at the interface between A and AB, for example, induces deficiency of B atoms in the compound AB phase near the A-AB interface. The deviations from the stoichiometry near A-AB interface is recovered by the diffusion of B atoms in the AB layer.

1.5 Ion Beams in Semiconductors and the Si-Ge Alloy System

Ion induced compositional disordering in semiconductor superlattice structures at moderately elevated temperatures have been found to facilitate the fabrication of photonic devices, planar lasers, wave guides and modulators [14,15]. This was the first time that ion mixing had demonstrated its technological usefulness. Most disordering schemes reported to date require high temperature annealing to promote compositional mixing in superlattices [16,17,18]. Such a high temperature process tends to restrict device fabrication because of the decomposition of the structures and possible reaction between metal mask and the substrates during annealing. The initial technological driving force was to form deep conducting layers in Si [24] and this application stimulated keen interest specifically in studying damage production by MeV ions and its removal by thermal

annealing [25,26], particularly in comparison with near-surface disorder produced in the more usual KeV range. At this time it was also realized that heavy MeV ion irradiation offered considerable control over energy deposition distribution and defect formation over large depths. These attributes were used to advantage for inducing epitaxial growth at low temperature [27,28] and as a means for studying solid phase epitaxial growth [29] and defect enhanced diffusion [30]. Technologically, MeV ion beams are used in specific Si processing steps [31], for isolating III-V devices [32], for disordering superlattices , forming optical wave guides and cavities [34] and improving electrical activation of deeply doped layers [31]. Topics of more fundamental solid state physics have been perused. These include studies of ion beam induced amorphization [35], crystallization [36]. MeV ions have also afforded the production of novel amorphous-crystalline materials [37].

Band gap engineering involving group IV semiconductor alloys has been the focus of recent research because of potential applications in modern electronics [20]. Ion beam mixing at moderately elevated temperatures may be useful in eliminating the high temperature step involved in annealing for compositional disordering. In recent years much interest has been focused on the Si-Ge alloys for use in high performance heterojunction bipolar transistor (HBT). These transistors have been fabricated using ultra high vacuum chemical vapor deposition (UHV-CVD) and molecular beam epitaxy (MBE) for the epitaxially grown SiGe layer and have promising device characteristics [19].

In accordance with the Home-Ruthery rule [39] Si and Ge form

a completely miscible solid solution across the entire compositional range [40]. The band gap of the Si-Ge system varies to give a wavelength range of 1.3μm to 1.5μm, making it suitable for fiber optical communication application. Multilayered films of a-Si and a-Ge have been made in the early eighties [41]. Interdiffusion in Si\Ge amorphous multilayer films [42] and thermally activated diffusion studies have also been carried out. Theoretical studies [43,44] have revealed the possible application of Si_xGe_{1-x} alloys in integrated wave guides [45], high speed 1.3μm detectors [46]. Photoluminiscence in Si-Ge superstructures [47] indicate the presence of quasi-direct band gaps, important for optical applications.

Matteson et al. [48] and Paine et al. [49] have studied the IBM of thin germanium markers in amorphous Si as a function of irradiation temperature. Liu et al. [50] have carried out compositional disordering and mixing in Si-Ge layered structure. Si-Ge layered structures have also been studied to investigate the kinetics of mixing using marker layers in amorphous silicon [51]. Chaudhari [52] has carried out mixing of this system at room temperature for various configurations and found definite evidence of mixing. Ramakrishnan [53] has studied the temperature dependence of mixing efficiency in Si-Ge bilayer structure, showing the existence of a thermal and an athermal region.

Keeping in mind the advantages of multilayers described earlier in this chapter we have undertaken the the study of ion beam mixing of Si-Ge multilayer structure in an effort to synthesize Si_xGe_{1-x} alloys at temperatures much less than the conventional methods of thermal diffusion and to characterize them, both optically and electrically.

'urther, bilayer configuration both at room and high temperatures have)een studied in detail [52,53]. This facilitates the comparison)etween the two configurations giving us a complete picture of this ;ystem.

Silicon and Germanium films in the thickness range of 250-350 A^{o} vere deposited sequentially on clean quartz substrate without any)reak in vacuum, forming multilayered structure with 6 to 10 films. Ion mixing experiments have been performed using 1 MeV Kr^{+} ions, doses (3-10) x 10^{15} atoms/cm^{2} using the 2 MeV Van de Graaff facility [54] at temperatures ranging from 25^{o}C to 300^{o}C. The samples were characterized using 1.3 MeV He^{+} for Rutherford Backscattering (RBS) Spectrometry.

Chapter 2 has the experimental details including sample preparation, ion beam mixing, characterization and the software packages used in simulations. The results and their analysis and discussion are presented in Chapter 3. Finally, the salient features and conclusions are stated in Chapter 4.

C H P T E R 2

EXPERIMENTAL DETAILS

;eneral

This chapter outlines the experimental arrangements made ınd procedures carried out during the course of investigation. The ;ssential details of sample preparation and characterization have been liscussed here.

?.1 Sample design

The use of multilayered films in ion beam mixing is capable ɔf producing alloy phases of desired composition. Fig 2.1. schematically shows the concept and arrangement of Ion Mixing using multilayered films.

The relative thickness of the layers are calculated using their atomic density. The thickness of the layers was decided on the basis of the energy resolution of the Rutherford backscattering set-up for 1.0 MeV to 1.4 MeV He^+beam. The sample design was thus based on the calculations made with the help of the simulation software TRIM and RUMP. The details of these software packages are mentioned later in this chapter.

The RUMP calculations estimated the minimum thickness required for the resolution for characterizing the sample with ion beams with energy ranging from 1.2 to 1.4 MeV. From the TRIM calculations the range of Kr^+ 1 MeV ion beam in SiGe alloy and the energy deposited by the incident projectiles to the target atoms was

obtained. The total thickness of the mutilayered structures for the ion beam experiments was selected on the basis of these calculated parameters in order to optimize the mixing. The parameters obtained are tabulated below.

Table 2.1 Estimated sample configuration for $Si_{.5}Ge_{.5}$ alloy

Thickness of each Si and Ge layer:	200 - 300 A^{O}
Total thickness of the multilayered structure	:3000 - 4000 A^{O}

The substrate used was SiO_2 for all the samples. This choice not only provided a transparent substrate for optical characterization but also it being an insulator helped in the electrical characterization by four probe method.

2.2 Transport and range of ions in matter (TRIM)

The theoretical calculations of krypton ion ranges and damage was performed using TRIM computer package developed by Ziegler et al.[57]. The nuclear energy deposited by the projectile ions to the target (Si-Ge multilayers) was calculated using this program. The program input consists of ion mass and energy, the details of the layer structure, the displacement energy of the lattice atoms (E_d) and the binding energy (E_b).The details are given in the the book by Ziegler [57]. If Z_1 and E_1 are the atomic number and the energy of the incident ion, Z_2 is the atomic number and E_2 the energy acquired by the target atom after a collision event with the incident ion, the following can be the consequences under different conditions:

Condition	Consequence
$E_1 > E_d$, $E_2 > E_d$	A vacancy results
$E_1 < E_d$, $E_2 > E_d$	E_2 is released in the form of phonons
$E_1 < E_d$, $E_2 > E_d$	Original atom remains at the site. The event is called a Replacement Collision
$Z_1 \neq Z_2$	Z_1 becomes an anti site atom
$Z_1 = Z_2$	Z_2 merely replaces Z_1 in the cascade and E_1 is released as phonons
$E_1 < E_d$, $E_2 < E_d$	Z_1 becomes an interstitial and $E_1 + E_2$ is released as phonons

The TRIM program has the provision of performing calculations for a maximum of 3 layered structure only. Therefore for a 10 layered sample like mine TRIM calculations are made by considering the overall composition of the structure so formed. Calculations were made by two methods. One was to give the relative composition of the elements as obtained from the multilayered structure in a single homogeneous layer of thickness of the total multilayer structure. The other method was to give an energy input to the first three layers followed by the next three layers for which the input was the average energy of the transmitted ions. Repeated calculations for various configurations ie. 3+3+2+2 layers, 2+3+2+3 layers etc. were compared. The transmitted ion energy fluctuated by around 5%. The value of the energy deposited in the layered structure when compared to the energy deposited in the homogeneous layer of appropriate composition was found to be

approximately identical at 110 eV/ion/angstrom (Fig 2.2a). The range o the krypton ions is shown in figure 2.2b. This gave the range and fina

istribution of the Krypton ions. During irradiation the energy of the on beam fluctuated by around 10%. So the values calculated thereof re accurate to only within 10%.

.3 Sample Preparation

Fused quartz was used as substrate for thin film deposition. he quartz was cut into pieces of size 10mm x 7mm each for Kr rradiations. They were cleaned using organic solvents such as TCE ollowed by a thorough rinse in acetone. The thin film deposition was arried out using an electron beam evaporation unit. Thermionic lectrons from a tungsten filament are bent using a permanent magnet and a high negative voltage to focus the electron beam onto graphite crucibles containing the material to be evaporated. These crucibles were mounted on a copper block to conduct away the heat rapidly. The advantages of e-beam evaporation over thermal evaporation are accurate control of the rate of deposition, no requirement to measure the mass of the material to be evaporated, better control over the deposited thickness and the ability to perform a number of evaporations of different materials without a break in vacuum. This is made possible by the use of rotating crucibles. The rate of deposition and therefore the thickness can be controlled by the current passing through the tungsten filament emitting thermionic electrons. Si and Ge films were alternately deposited onto a clean quartz substrate in a vacuum of the order of 10^{-5} torr. The sample consisted of 6-10 layers all deposited without a break in vacuum.

2.4 Heavy Ion Irradiation

Krypton ions of energy 1.0 $\pm$ .05 MeV generated by the accelerator was used to irradiate the samples with doses ranging from $3x10^{15}$ to $5x10^{16}$ atoms/cm^2. The beam spot of the ion beam was typically of 4mm x 5mm size. The irradiation was carried out at substrate temperatures from 25^{O} to $260^{O}C$.

The ion bombardments on $Si/Ge/SiO_2$ samples were carried out in the heavy ion irradiation chamber Fig.2.3. The chamber is mounted on a Turbo Molecular pump. This can provide vacuum up to 10^{-6} torr. It has a movable sample holder with the help of which a number of samples can be irradiated without any break in vacuum. The holder is electrically isolated by a perspex flange. A current integrator connected to the sample holder measures the total charge acquired during irradiation. The current integrator can be preseted for a value of collected charge. As soon as the deposited charge equals the preseted value a signal is generated which is given to a electronic circuit to close a shutter in the path of the ion beam. In this way irradiation for a predetermined value of a dose can be performed. Surrounding the sample holder is a suppressor arrangement which is a cylinder made of Aluminum sheet kept at a potential of nearly -260V relative to the grounded chamber. This inhibits the emission of secondary electrons from the sample during Krypton ion implantation, preventing the interference of secondary electrons with the measurement of total charge. The beam entering the chamber is collimated by the X-Y slits and is further collimated by an aperture mounted just before the sample holder [52]. The irradiations were carried out using low ion current density between .1 to .2 $\mu A/cm^2$.

2.4 Heavy Ion Irradiation

Krypton ions of energy 1.0 $\pm$ .05 MeV generated by the accelerator was used to irradiate the samples with doses ranging from $3x10^{15}$ to $5x10^{16}$ atoms/cm^2. The beam spot of the ion beam was typically of 4mm x 5mm size. The irradiation was carried out at substrate temperatures from 25^{o} to $260^{o}C$.

The ion bombardments on $Si/Ge/SiO_2$ samples were carried out in the heavy ion irradiation chamber Fig.2.3. The chamber is mounted on a Turbo Molecular pump. This can provide vacuum up to 10^{-6} torr. It has a movable sample holder with the help of which a number of samples can be irradiated without any break in vacuum. The holder is electrically isolated by a perspex flange. A current integrator connected to the sample holder measures the total charge acquired during irradiation. The current integrator can be preseted for a value of collected charge. As soon as the deposited charge equals the preseted value a signal is generated which is given to a electronic circuit to close a shutter in the path of the ion beam. In this way irradiation for a predetermined value of a dose can be performed. Surrounding the sample holder is a suppressor arrangement which is a cylinder made of Aluminum sheet kept at a potential of nearly -260V relative to the grounded chamber. This inhibits the emission of secondary electrons from the sample during Krypton ion implantation, preventing the interference of secondary electrons with the measurement of total charge. The beam entering the chamber is collimated by the X-Y slits and is further collimated by an aperture mounted just before the sample holder [52]. The irradiations were carried out using low ion current density between .1 to .2 $\mu A/cm^2$.

For higher temperature irradiation, the sample holder is odified. It is made of high purity copper for good thermal onduction. The sample holder is isolated from the chamber by means of ceramic insulator to prevent heat loss from the irradiation chamber. 'he heating arrangement consists of a tungsten filament lamp of high :urrent rating (25V,10A). A reflector of stainless steel sheet is used .o focus the light on the sample holder and to prevent the chamber /alls from heating by radiation. A chromel-alumel thermocouple junction was placed on the substrate between mica sheets to measure ind control the temperature with the help of a Indotherm temperature :ontroller within $\pm 3^{o}C$. With the above arrangement temperatures as high is $330^{o}C$ were reached.

It was observed that during heating, when the current :hrough the heater was more than 3A, the charge meter showed a :onstant current even in the absence of the ion beam. This can be attributed to the leakage current. Therefore, a charge measurement system independent of the sample holder was used. This works on the principle of the vibrating reed in the path of the ion beam. The current due to the ion beam falling on the reed is a measure of the dose.

2.5 Annealing

Ion beams incident on the sample cause radiation induced damage of the irradiated portion. It is necessary from device technology view point to remove this damage. Annealing of samples were carried out in a clean quartz tube in flowing dry nitrogen gas environment. Temperature control was achieved by using an Indotherm

emperature controller with the ability to control within $\pm 3^{o}C$. The emperature measurement was made using a calibrated chromel-alumel hermocouple. The annealed samples were used to characterize the amples electrically and optically. Annealing was carried out at $620^{o}C$ or 15 minutes.

:.6 Ion Beam Analysis

Fig.2.4 gives the details of the RBS chamber. This chamber .s mounted on a diffusion pump vacuum system with a liquid nitrogen .rap which yields a vacuum of the order of 10^{-6}torr. The samples are ıounted on a sample holder similar to the one used in the heavy ion ırradiation chamber. A suppressor and a similar charge measuring ɜlectronics is used.

The Helium ion beam is collimated before entering the RBS chamber ɔy a X-Y slit arrangement to obtain a beam spot of about 1mm x 1mm ɟimensions. The detector is mounted at a scattering angle of 150^{o} and subtends a solid angle of 2.57 millisteradian at the center of the ɔeam spot. The silicon surface barrier detector is mounted on a cylinder cooled by the circulation of chilled water. This helps in the reduction of the leakage current in the surface barrier detector from 200nA to 50nA. The detector is kept at a bias of +100V. The

electrical signals from the surface barrier detector are analyzed by the usual nuclear electronics and multichannel analyzer. The height of the signal gives the energy of the detected particle. A plot of the energy of the particles versus the frequency of occurrence of the signal is called as a "spectrum" which contains the information regarding the elements and their depth distribution in the sample. In

.hese measurements an EG&G ORTEC 142A preamplifier, 572 Amplifier and gated biased amplifier an ND65 PC multi channel analyzer connected to a PC were used.

2.7 RBS and the RUMP Simulation Package

Ion beams can be used for both material modification and analysis. The text by Feldman gives a comprehensive introduction to some common analysis techniques using ion beams [58]. The Rutherford Backscattering technique is one of the most frequently used techniques for quantitative analysis of composition, thickness and depth profiles of thin solid films or solid samples near the surface region. Due to it's simplicity, versatility and amount of information it can derive in a short data acquisition time it has evolved in the past few years into a major materials characterization tool.

The basic requirements for an RBS measurement is given in the Fig. 2.5. The requirement for RBS are :

1. A particle accelerator to provide required energetic charged particles eg. 2 MeV Van de Graaff accelerator.
2. An ion source which provides ions of desired gaseous species.
3. A scattering chamber described above
4. A computer simulation package to analyze the data.

In this work the DOS package RUMP has been used for analysis

The RUMP simulation program has been developed at the Cornell university by Doolittle and co-workers [59] .In the simulation, a theoretical sample structure consisting of several

ayers of varying thickness is first prepared . The experimental)arameters are fed in to the program. A backscattering spectrum thus :onstructed is compared with the experimental spectrum. This procedure ls used iteratively to arrive at the best set of parameters so that :he simulated spectrum compares well with the experimental data. For :he work in this thesis it was required to simulate the structures of 3i-Ge multilayer systems. The backscattering spectra for a Si-Ge as evaporated sample is shown in Fig.2.6 along with the theoretical layer structure.

2.8 Optical Characterization

The knowledge of the absorption coefficient as a function of wavelength of a material is necessary to determine the optical band gap of that material. The practical situation for a thin film on a transparent substrate is shown in Fig. 2.7The film has a thickness d and and absorption coefficient α. The transparent substrate has a thickness several orders of magnitude larger than d and absorption coefficient 0.

The transmission T is a function of wavelength, thickness, refractive index and absorption coefficient of both the sample and the substrate. The refractive index of air is taken to be 1. Films with uniform thickness give rise to interference fringes as shown in Fig 2.8. The interference transmission T_α can be obtained by the relation

$$T_\alpha = (T_M T_m)^{1/2}$$

here T_m and T_M are the extremes of the interference fringes orresponding to a wavelength λ and the values are obtained by drawing n envelope of the extremes of the transmission spectra.

From the transmission spectra the absorption coefficient as function of wavelength can be obtained by the following relation

$$\ln\left(\frac{I_1}{I_0}\right) = -\alpha d$$

here I_2 is the intensity at that wavelength for transmission through ir and I_1 for transmission through sample. A plot of $(\alpha h\nu)^{1/2}$ vs $h\nu$ ives the band gap on extrapolation of the graph form the point of hange of slope [60].

The schematic diagram of the experimental set up used is iven in figure 2.9. The monochromator consists of a diffraction rating. The transmission is measured in terms of the potential drop cross a 1MΩ resistor. A chopper is used to negate any effect of he surrounding illumination. A Si detector is used for wavelengths

rom 400 nm to 1100 nm after which a Ge detector is used for avelengths up to 1200 nm.

2.9 Resistivity Measurements

The sheet resistance of a semiconductor is an important often measured parameter. The most commonly used technique in the semiconductor industry for measuring resistivity is the "four point probe method" [61]. This method is nondestructive, speedy and does not involve any elaborate preparations. The four point probe comprises

four equally spaced metal probes which are in contact with the semiconducting surface. The probes are at the corner of a square, allowing a smaller geometry like that of our samples. in our arrangement the probes are at the corners of a 3mm x 3mm square.

If the ratio of the layer thickness (X) to the probe spacing (S) is less than 0.4 then the average resistivity of an infinitely thin sample in which the current flow is parallel to the surface is given by :

$$\rho = \left(\frac{\pi}{2 \ln 2} \frac{V}{I} \right) X = 2.266 \frac{V}{I} X \quad \ldots \text{ for square probes}$$

The above formula [1] can be used to calculate the resistivity of wafers and diffused and implanted layers. The current flows through the adjacent probes and the voltage is measured across the other two.

C H A P T E R 3

RESULTS AND DISCUSSIONS

General

The results of the Rutherford backscattering spectroscopy, nd the optical and electrical characterization are reported and iscussed in this chapter. There are two configurations of the ıultilayered structure deposited on quartz substrates that have been ısed. Configuration 1 consists of three alternate layers of Si and Ge :ach with a total thickness of 2700 A°with a nominal composition ratio ;i$_4$Ge$_5$. Configuration 2 similarly has five alternate layers with a .otal thickness of 3200 A°with a nominal composition of Si$_5$Ge$_6$. The lose dependence study at room temperature and at higher substrates .emperatures up to 300°C will be presented and discussed along with :he results of resistivity and transmission measurements.

3.1 RBS Measurements and Results

3.1.1 A typical RBS spectrum of a multilayered structure

Fig. 3.1 shows a typical RBS spectrum for a multilayered sample ıaving 5 layers each of Si and Ge with the simulated spectrum on quartz substrate with Si as the top layer. The deposition was

performed to achieve thickness of individual Si and Ge layers of 300 A°each. The actual thicknesses of these layers as obtained from the RBS analysis is given later . It showed a variation up to 30% from the expected configuration. The surface positions of Ge, Si and O are shown by arrows in this figure. The RBS signals from Ge start from channel no 476 and extend to 328 while the Si signals starts at a lower channel no. of 290. The lower energy edge of the signal from Si is not distinct as it overlaps with the signal from the substrate which consists of Si and O. Thus the signals from Ge layers are well separated from Si due to the large separation in their atomic masses. The RBS signals from oxygen present in the multilayer structure rides over the continuous background of the substrate. The Ge signals consists of 5 sharp peaks. Similarly Si also exhibits 5 peaks. These individual peaks belong to the individual Ge/Si layers. Thus the first Si peak (channel no.290) and the first Ge peak (channel no.476) correspond to the top Si Ge pair of the configuration. The separation between two Ge peaks arises from the presence of a Si layer in between. Nevertheless, there is an overlap between two consecutive peaks of Ge due to the finite detector resolution (13 KeV equivalent to a depth resolution of 100 A° for Ge).

3.1.2 CONFIGURATION 1: SIX ALTERNATE LAYERS OF SI AND GE ON QUARTZ SUBSTRATE.

The RBS spectrum of the as-evaporated sample along with the simulated spectrum is shown in Fig. 3.2. The simulated spectrum shows a good visual fit to the experimental spectrum suggesting that the layer structure used in the simulation represents the actual sample structure.

Table 3.1 The configuration of the sample on quartz substrate as revealed is ·

Layer no.	Thickness (A^O)	Composition		
		Ge	Si	O
1	870	1.00	-	-
2	470		0.75	0.25
3	310	0.953	-	0.047
4	430	-	0.905	0.095
5	380	0.909	-	0.091
6	300	-	0.909	0.091
7	30000	-	1	2

The corresponding geometry is shown in the figure for easy visualization of the sample structure.

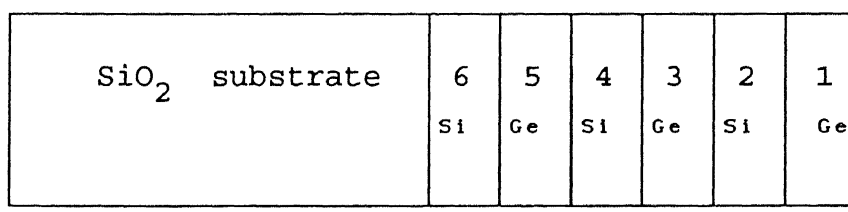

Fig. 3.3

It may be noted that the top layer of Ge in this case is very thick than the expected thickness.This configuration was used to study the dose dependence of mixing at room temperature. The presence of oxygen in the sample as evident from the sample structure obtained from simulations using RUMP can be attributed to the presence of oxide on the surface of the Si and Ge pellets used during thin film deposition. The presence of oxygen could influence the mixing process. However, in an earlier report Desimoni et al. [64] have shown that the presence of oxygen has no effect on mixing of Pd/Si system.. Further, they have shown that irradiation with 80 KeV Ar ions resulted in the dispersal of oxygen atoms from the contaminated layers resulting in

nhindered mixing. In fact a more energetic beam should be even more fficient for the dispersal [63]. Thus in accordance, we expect that he presence of oxygen in our sample will not affect the mixing of i/Ge.

The simulation analysis also shows that there is no interfacial nteraction between various layers. The RBS spectra showing the effect f 1 MeV Krypton ion irradiation on the above sample for various doses long with their simulated spectra are shown in the figures 3.4, 3.5, nd 3.6. The results of TRIM calculations is shown in Fig.3.7.

The simulation structures used for the different doses are iven in Tables 3.2, 3.3 and 3.4 From the RBS spectrum analysis of fig .2 we note that mixing has occurred at all the interfaces. The top hick layer of Ge has an unreacted thickness of 500 A°. This implies hat the Si atoms have come up to a distance of 300 A°from the nterface into the Ge layer . This is in accordance with the bservations reported for the bilayer structure [52]. Note that the expected composition after complete mixing would have corresponded to $Si_{0.44}Ge_{0.66}$. There is very little difference in the relative composition of Si and Ge in different layers obtained after mixing for the dose 3×10^{16}at/cm^2. For a higher dose of 5×10^{16}at/cm^2 the thickness of the unreacted top Ge layer has decreased considerably. From the bilayer results [52] it is seen that for high doses of 5×10^{16}at/cm^2 Si

diffuses into Ge up to 600°A across the interface. For lower doses the distance travelled by the Si atoms across the interface is about 300 A°. Thus, it is in agreement with the results obtained for the bilayer configuration. In general alternate Ge and Si rich layers are found to have been synthesized. From the TRIM calculation (Fig 3.7) we see that the average energy deposited is 120 eV//ion/A over the entire thickness range. Thus the mixing at all the interfaces can be explained. Fig. 3.8 shows a comparison of mixing occurred with $5x10^{16}$at/cm^2 with the as evaporated sample.

Table 3.2 Structure of the sample after irradiating with Kr ions with a dose of $2x10^{16}$at/cm^2. The thickness is in A°.

Layer	Thickness	Composition		
		Ge	Si	O
1	500	1	-	-
2	300	0.9	0.1	0.1
3	400	0.2	0.7	0.1
4	280	0.5	0.5O	0.02
5	500	0.3	0.7	0.1
6	320	0.6	0.4	-
7	320	0.2	0.74	0.06
8	30000	.	1	2

Table 3.3 Structure of the sample after irradiating with Kr ions with a dose of 3×10^{16} at/cm^2. The thickness is in A^0.

Layer	Thickness	Composition		
		Ge	Si	O
1	500	1	-	-
2	300	0.9	0.1	0 .1
3	420	0.25	0.65	.08
4	280	0.5	0.5	-
5	500	0.3	0.7	0.1
6	300	0.6	0.4	-
7	300	0.2	0.8	0.1
8	30000	-	1	2

Table 3.4 Structure of the sample after irradiating with Kr ions with a dose of 5×10^{16} at/cm^2. The thickness is in A^0.

Layer	Thickness	Composition		
		Ge	Si	O
1	80	1	-	-
2	580	0.9	.1	-
3	140	0.8	0.2	-
4	160	0.7	0.3	0.1
5	440	0.3	0.7	0.05
6	270	0.5	0.5	0.1
7	380	0.3	0.8	-
8	410	0.55	0.5	0.1
9	300	0.2	0.7	0.1
10	30000	-	1	2

.1.3 CONFIGURATION 2 : TEN ALTERNATE LAYERS OF Si AND Ge ON QUARTZ SUBSTRATE.

The RBS data obtained along with the simulated curve for the as vaporated sample is shown in Fig. 3.1. Since the simulated spectrum ives a good visual fit to the experimental spectrum, we can herefore, roughly estimate the sample configuration . The sample onfiguration used in the calculations is given in table 3.5.

able 3.5 Sample configuration of the 10 layered sample.

The thickness is in A^0.

Layer	Thickness	Composition		
		Ge	Si	O
1	170	-	1	1
2	240	1	-	-
3	290	-	1	0.15
4	320	1	-	-
5	350	-	1	0.21
6	350	1	-	-
7	320	-	1	0.27
8	310	1	-	-
9	500	-	1	1
10	330	1	-	0.1
11	30000	-	1	2

he sample geometry of the 10 layered sample is shown below

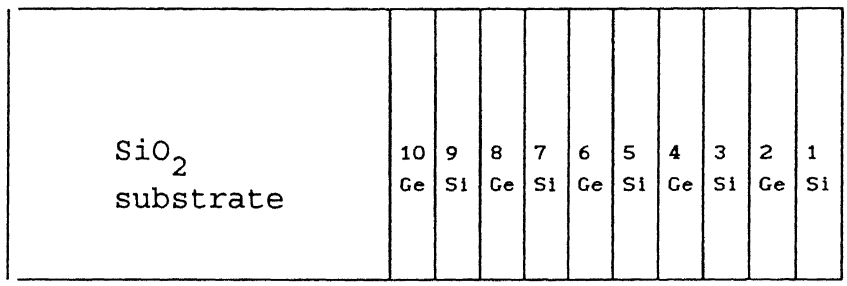

Fig 3.9

It may be noted that the top layer of Si in this sample has ı high concentration of oxygen. This could be because of Silicon's .endency to form an oxide very readily. As discussed in the previous section, the presence of oxygen atoms does not effect the ion beam mixing as the oxygen atoms get dispersed because of ion bombardment. This sample was used to investigate the effect of high temperature irradiation on mixing at a single dose of 1×10^{16} at/cm^2.

The RBS spectra showing the effect of 1 MeV Krypton ion irradiations at room temperature and high substrate temperature along with the simulated spectra are shown in Figures 3.10, 3.11, 3.12 respectively. The results of TRIM calculation are shown in Fig 3.13.

The structures obtained from the simulation analysis are given in Tables 3.5, 3.6 and 3.7.

From Table 3.5 we note that mixing does not occur at the first interface (from the top layer) and the last interface of Si and Ge. Also the mixed layer of composition $Si_{.5}Ge_{.5}$ is sandwiched between elemental Si and elemental Ge layers. It may be noted that the final composition of the configuration on complete mixing would have yielded the composition of $Si_{0.55}Ge_{0.45}$ Mixing at higher temperatures of 200°C and 250°C show mixing at all the interfaces. However, layers of unreacted Si and Ge are present up to a depth of 1600 A°below which there is no unreacted layer. Thus mixing between the layers increase beyond a depth of 1600 A°for samples whose substrate temperatures were 200°C and 250°C. The thickness of the unreacted Si and Ge layers do not change considerably with a rise of 50 °C in temperature. Whereas there is a rise in the mixing observed with temperature, it shows the same mixing at temperatures 200 and 250°C.

To study the temperature dependence mixing, irradiations were carried out for substrate temperatures of 300°C. Contrary to the expected Arrhenius behavior, the mixing shows a decline as compared to the mixing occurring at 200°C and even room temperature for the same dose. Comparison of the spectrum obtained for the sample irradiated at 300°C with the as evaporated spectrum (Fig. 3.14) shows a decrease in

he trough and peak heights indicating the occurrence of mixing. When he spectrum is compared with the one obtained for room temperature rradiations, we observe a reduction in mixing (Fig. 3.15). This esult is surprising. However, in the room temperature irradiations carried out for the bilayer samples by Chaudhari [52] it has been eported that the growth rate at higher doses ($5x10^{16}$at/cm^2) is considerably retarded. Such retardation at high temperatures is indeed quite surprising. The reasons for such retardation and the underlying mechanisms of inhibition of growth is not clear and needs to be investigated in detail.

From the TRIM calculations (Fig. 3.13) the energy deposited by the incident projectile to the target atoms from Fig 3.12 clearly shows a rise in the energy deposited with depth. Approximately at a depth of 1200 A^O the energy deposited becomes constant up to the interface between the substrate and the last layer. This constant energy is ~ 120 eV/ion/A^O. This effect of the increase in the energy deposited from the surface up to a depth of 1200 A^O can be seen in the pattern of mixing that has taken place. The reduction in the peak to trough ratio is significant beginning from the sixth deposited layer which is at a depth of 1250 A^O. Figures 3.16, 3.17, 3.18 compares the mixing occurring at room temperature, at 200^{O}C and 250^{O}C with the as

vaporated sample.

able 3.6 Sample configuration after irradiation with $1x10^{16}at/cm^2$ at room temperature. The thickness is in A^0.

Layer	Thickness	Composition		
		Ge	Si	O
1	170	-	1	0.5
2	220	1	-	-
3	20	0.5	0.5	-
4	290	-	1	0.08
5	85	0.5	0.5	-
6	230	1	-	-
7	90	0.5	0.5	-
8	250	-	1	0.21
9	150	0.5	0.5	-
10	160	1	-	-
11	130	0.5	0.5	-
12	170	-	1	0.27
13	130	0.5	0.5	-
14	180	1	-	-
15	70	0.5	0.5	-
16	460	-	1	1
17	320	1	-	.1
18	30000		1	2

Table 3.7 Sample configuration after irradiating at 200^{O}C with a dose of 1x10^{16}at/cm^{2}. The thickness is in A^{0}.

Layer	Thickness	Composition		
		Ge	Si	O
1	140	-	1	0.5
2	30	0.5	0.5	-
3	200	1	-	-
4	60	0.5	0.5	-
5	210	-	1	0.08
6	120	0.5	0.5	-
7	190	1	-	-
8	130	0.5	0.5	-
9	190	-	1	0.21
10	250	0.5	0.5	-
11	100	1	-	-
12	160	0.5	0.5	-
13	170	0.3	0.7	0.27
14	220	0.5	0.5	-
15	100	0.7	0.3	0.1
16	190	0.5	0.5	0.1
17	360	0.3	0.7	0.8
18	150	0.5	0.5	0.1
19	250	0.7	0.3	0.1
20	30000	-	1	2

able 3.8 Sample configuration after irradiating at 250^{O}C with a dose of 1x10^{16}at/cm^{2}. The thickness is in A^{0}.

Layer	Thickness	Composition		
		Ge	Si	O
1	100	-	1	0.4
2	40	0.5	0.5	-
3	170	1	-	-
4	100	0.5	0.5	-
5	210	-	1	0.08
6	130	0.5	0.5	
7	180	1	-	0.05
8	140	0.5	0.5	-
9	170	-	1	0.21
10	260	0.5	0.5	-
11	90	1	-	0.2
12	160	0.5	0.5	0.1
13	90	0.3	0.7	0.4
14	60	0.35	1	0.15
15	200	0.5	0.05	0.1
16	140	0.8	0.3	0.15
17	170	0.5	0.5	0.2
18	250	0.3	0.7	0.65
19	170	0.5	0.5	0.05
20	270	0.7	0.3	0.1
21	30000	-	1	2

3.2 MIXING MECHANISM

It is known that for bilayer configuration the mixing efficiencies for a number of systems show thermal and a athermal regime of mixing. There is a characteristic temperature T_c below which the mixing is independent of temperature. In this regime mixing is induced by the following processes :

(i) Recoil implantation

In this, as the incident ion penetrates the target, it makes some high energy collision with target atoms, and these atoms recoil far from their initial locations. The number of high energy collisions is small as the cross section for the high energy collision is small. This process is independent of temperature.

(ii) Cascade mixing

As the cascade develops in time, secondary recoil atoms are displaced and they in turn displace other atoms. The initial momentum of the incident particle is soon lost and the cascade becomes isotropic. The cascade formation is illustrated in fig. 3.19 and 3.20.for 100 KeV and 1MeV krypton incident on Si/Ge bilayer structures.Note that for the lower energy of 100 KeV when the Ge film is on the top of the sample the collisions almost result into a single cascade. For a high energy beam we see non overlapping cascades called the local cascades along the path of the ion. Further the local cascade overlap is more prominent in Ge than in Si.

The cascades when developed in a limited volume inside a solid with the majority of atoms temporarily in motion, thermal spike is observed. It is said that the atomic motion has reached a state of quasi-equilibrium. The questions regarding the culmination of the collision cascades into a spike, the energy density of the spike etc. have been explained on the basis of the novel approach of fractal geometry of the collisions by Cheng and others [67,68]. For a space filling cascade a spike can occur when the interaction potential is characterized by a $V(r) \alpha r^{-1/m}$ with $0 < m < (1/6)$. In reality these potentials correspond to a kinetic energy in the hundreds eV to eV range. Critical energy E_c is the energy at which the inverse power potential takes the exponent $m = 1/6$. This energy is a characteristic of the atomic number and it decreases with Z. For $Z < 20$ its value goes down below the typical displacement energy E_d= 30eV. The spikes are not expected to occur for pure elemental solids with Z<20. Thus, in the Si/Ge system, spikes are not expected to form in the Si layers. However, as the mixing proceeds, with the migration of Ge and Si atoms across the interface, spikes would form in all layers. Cheng [67] has also calculated theoretically the dose dependence of the mixing for diffusion in cascade and thermal spike. The square of the mixed thickness shows a linear dependence on the dose and the deposited energy F_d for cascade mixing and a non linear dependence for mixing by

hermal spike .

The earlier results from bilayer configurations [52,53] show an nitial linear dependence of mixing followed by a non linear lependence of mixing on dose. This is in accordance with the predictions made above that for SiGe layered structure the mixing via hermal spike should occur at higher doses. From the temperature lependent studies of mixing of bilayer samples Ramakrishnan [53] has reported that the critical temperature of this system is 205°C above vhich the mixing becomes temperature dependent. In accordance with this observation we also find that higher degree of mixing leading towards homogeneous composition occurs at 200°C and 250°C as compared to room temperature for similar irradiation fluences.

So far, most of the work carried out in multilayer and bilayer nixing has been essentially devoted to metal/metal and metal/semiconductor system. The models and mechanisms proposed may be applicable to the Si/Ge ie. semiconductor/semiconductor system. Si/Ge system is unique as compared to the above mentioned systems as it is the only elemental semiconductor/semiconductor system. Interestingly, although it forms a solid solution across the entire compositional range, under the irradiation conditions and it goes into a highly disordered state at room temperature.For alloy formation in ion beam mixing several phenomenological models have been proposed. Liu et al.[13] have proposed a "structural difference rule" to predict the

ıture of the mixed alloy. According to this rule ion beam mixing of ɪements having different crystal structure result into the formation ɛ an amorphous alloy when the alloy composition lies in the two phase ɐgion of the phase diagram. For elements with different crystal ɛructure but with composition in the single phase region of the phase iagram and for elements having same crystal structure metastable or table crystalline phases result. On the basis of this rule Si/Ge ystem should form a crystalline alloy since both have same crystal tructure and they form a continuous solid solution. However, in ontrast, we find that a homogeneous alloy formation does not take ɔlace even at the highest dose for the multilayer structure. This ıight be due to the fact that both Si and Ge go into a highly lisordered state under irradiation. According to phenomenological ıodel proposed by Johnson et al. [67], ion mixing can be treated as a andom walk in the athermal regime. This model applies specifically in ell developed cascades where the particles are thermalizing after the ɪncident ion and secondary ions lose most of their energies in about 10^{-13}sec. In this model the mixing parameter depends on the heat of ıixing and the cohesive energy of the system. For a bilayer the mixing ɔarameter is given by

$$\frac{Dt}{\phi} = \frac{1}{4\rho^2} \frac{K_1 \varepsilon^2}{(\Delta H_c)^2} \left[1 + K_2 \frac{\Delta H_m}{\Delta H_c} \right]$$

where K_1 and K_2 are constants, ε is the energy deposited per unit path length, ρ is the average atomic density, ΔH_c is the cohesive energy of the system and ΔH_m is the heat of mixing. On examining the above equation we see that ΔH_m represents the driving force of mixing and ΔH_c represents the resistance to mixing. It has been reported that a mismatch strain exerts a biasing force to enhance mixing in the athermal regime in case of bilayers [68]. For samples with multiple strained layers, the enhancement of mixing can be larger due to larger biasing force in this type of structures.

It has been noted that the mixing rate in the athermal regime appears to be faster for epitaxial samples prepared by Molecular Beam Epitaxy (MBE) than for amorphous samples prepared by e-beam evaporation. The Si/Ge system shows much less mixing as compared to mixing observed in other systems. This can be attributed to the amorphous nature of the films and the fact that the heat of mixing is small and cohesive energy is high for the system. Further since the system is remaining amorphous the thermodynamic parameters are not aiding the mixing process.

We have not observed any significant difference in mixing for the irradiation temperature of 200°C and 250°C.(Fig.3.21) Interestingly, at 300 °C we have seen a reduction in the mixing across the interfaces. This suggests that there is a demixing phenomena occuring

at this temperature due to the change in defect mobilities and strain relaxation. However in order to completely understand the underlying phenomena measurements over a wide temperature range up to 900°C, at which the crystallization of Si/Ge occurs, have to be performed. On the basis of the arguments given above, we feel that a uniform composition is possible to obtain by ion beam mixing of Si/Ge multilayers at irradiation temperatures about 900°C. It may be noted that this temperature is still much lower than the one required to synthesize thermally a homogeneous SiGe alloy.

In summary, the krypton ions induce mixing over the entire multilayer structure giving rise to a variable SiGe composition across the depth. However uniform mixing is not observed under the presently used parameters.

3.3 Transmission Spectroscopy

A typical spectrum obtained is shown in figure 3.22. The presence of interference fringes indicates the uniformity of the film deposited. The measurements were performed after annealing the samples at 620 °C. Subsequent X-ray measurements showed that the samples are in a highly disordered state.The energy dependence of absorption coefficient allows us to determine the semiconductor band gap value and the nature of optical transition. The following relations are well known.

$$\alpha = B(h\nu - E_g)^{1/2} \quad \text{for direct gap semiconductor}$$

$$\alpha = B(h\nu - E_g \pm E_p)^2 \quad \text{for indirect gap semiconductor}$$

The high values of α (~ 10^4 cm^{-1}) are characteristic of the direct allowed transitions [65]. To obtain the band gap α^2 vs. $h\nu$ is plotted. It is well known that the absorption coefficient values satisfy the above given equations in a very narrow energy range [66]. Thus only a few experimental points obey the above mentioned relation. A typical plot of α^2 vs. $h\nu$ is shown in figure 3.23 On extrapolating the straight line we get the band gap of the material from the x-intercept. The band gap obtained for all the samples irrespective of their irradiating condition was of the order of 0.8 eV. This result could be explained by considering the fact that the samples examined consisted of Si_x Ge_{1-x} of variable composition over the entire depth. Also the mixed regions are in a highly disordered state.Because of this a number of direct transitions can occur. No change in the band gap can be explained by considering the dominance of tail end mixing in the density of states in the disordered structure.

3.4 Resistivity Measurements

The resistivity measurements were made to study the effect

of dose is shown in Fig 3.24. There is a lowering of resistivity after the annealing of the samples. The resistivity shows a sharp decline from the as evaporated sample to the irradiated sample after annealing at 620^{o}C in an inert environment of dry flowing Nitrogen for 15 minutes. However, the annealed samples do show a systematic increase in the resistivity with increasing dose. The significant decrease in the resistivity after annealing is an indication that damage has been recovered. Nevertheless, the dose dependence of resistivity of the annealed samples show that the significant disorder is still present in the sample. It is noteworthy that the damage recovery has occurred using significantly lower temperature and relatively short time.

The substrate temperature dependence of room temperature resistivity is illustrated in Fig 3.25. One observes that for the same dose and annealing conditions, there is a fall in the resistivity measured at room temperature with increasing substrate temperature. This feature is in addition to the fact that there is a fall in resistivity after ion irradiation and annealing. The fall in resistivity with increasing substrate temperature is in agreement with the fact that high temperature irradiation has the advantage of in situ annealing of defects produced during irradiation.

One of the consistent features of sheet resistivity measurements is that the as deposited layers have higher resistivities

than the ion irradiated ones. This clearly indicates that the as evaporated layers are initially more disordered and ion irradiation helps in relaxing the amorphous layer which is in agreement with the discussion made above in connection with the mixing mechanism. In the relaxed structure there is a higher possibility of electrical activation of shallower impurities giving rise to lower resistivity.

CHAPTER 4

SUMMARY AND CONCLUSIONS

There is a renewed interest in the Si-Ge system due to its possible applications in optoelectronic technology. Ion beam mixing can provide a powerful method for synthesizing Si-Ge alloy of desired composition on a preselected region of a sample at considerably low temperatures. In order to synthesize mixed Si_xGe_{1-x} layers of graded or uniform composition, ion beam mixing of multilayer configuration is a unique method which has not been explored. In view of this, in this study, ion beam mixing in multilayered sample configuration was undertaken to synthesize an alloy of predetermined composition and to study its optical and electrical characteristics.

Alternate films of Si and Ge were deposited on quartz substrate in high vacuum to yield mutilayered structure of 6-10 films each of thickness 250-350 A^{o}. Mixing experiments were performed using Krypton ions of energy 1.0 MeV. The irradiation dose was varied from $8x10^{15}$ to $5x10^{16}at/cm^{2}$. The irradiations were carried out at irradiation temperatures from Room Temperature to $300^{o}C$. The samples were characterized using Rutherford backscattering spectrometry , Transmission spectroscopy, four point probe and XRD measurements. Detailed simulations of the RBS spectra were carried out to investigate the change in the layer structure due to irradiation. The main conclusions of this study are listed below

1. The mixing at room temperature shows mixing across all the layers of the multilayer structure resulting into a variable composition of $Si_x Ge_{1-x}$ over the entire thickness of the multilayer. From the TRIM calculations mixing across the total multilayer thickness is also expected. The mixing occurs via cascades in the beginning while mixing thermal spikes dominate at higher doses.

2. Considerably enhanced mixing at high temperatures has been observed when compared to the mixing occurring at room temperature. However, the mixing occurring at 200^0C and 250^0C are the same. At 300^0C the mixing trend is reversed resulting into much lower mixing as compared to the mixing at 200^0C.

3. The enhancement of mixing at 200^0C ia attributed to the radiation enhanced diffusion occurring at this temperature which is just near the critical temperature for this system.

4. The saturation of mixing at 250^0C and retardation at 300^0C shows the effect of demixing which is competing the mixing process above 200^0C. The demixing can result from the strain relaxation due to ion irradiation and the highly disordered nature of the film.

5. The phenomenological models, which consider the energy deposition, the dose and the thermodynamic properties,proposed for metal/metal and metal/semiconductor systems are not completely applicable to the Si/Ge system because under irradiation both the elements remain in amorphous state. Under this condition the thermodynamic properties like cohesive

energy, heat of mixing etc. can't be utilized. Nevertheless, the small heat of mixing value and large cohesive energy for crystalline composition suggests a slow mixing process which agrees with our observation.

6. The XRD measurements show that the as evaporated, irradiated and annealed (620^{0}C for 15 min) are in a highly disordered state.

7. The value of the band gap is ~0.8 eV irrespective of the irradiating conditions.Since the multilayers remain amorphous even after annealing tail end mixing dominates as far as the band gap is concerned.

8 The resistivity measurements show that a low temperature heat treatment is enough to improve the conductivity of the sample indicating the removal of most of the ion induced damages. However, complete recovery of the damage has not occurred as it is evident from the increase in resistivity with dose.

9. A definite evidence of in situ annealing of defects is seen in the form of the decrease in resistivity with increase in substrate temperature for the same dose.

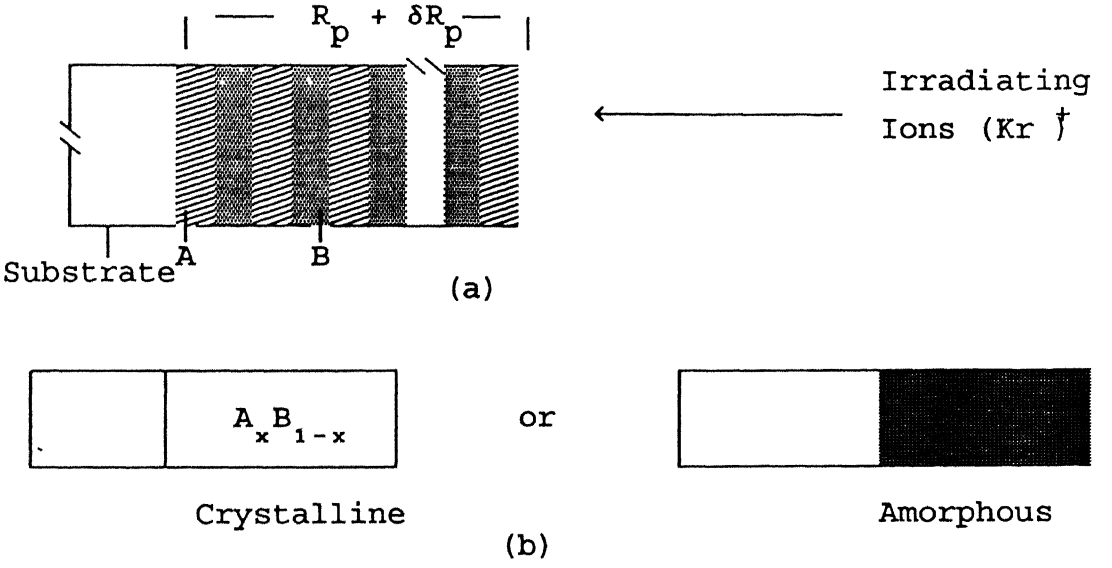
$R_p + \delta R_p$
Irradiating
Ions (Kr $^+$)
Substrate
A
B
(a)
$A_x B_{1-x}$
or
Crystalline
Amorphous
(b)

Fig 2.1

TRIM 92

ION TYPE	Kr^{+}
ION ENERGY	1 MeV
ION ANGLE	0 Deg.

Target layers	Depth
$Si_{.5}Ge_{.5}$	1 μm

IONS COMPLETED 3000

	Range (A)
Longitudnal	4795
Lateral Projection	1023
Radial Projection	1599

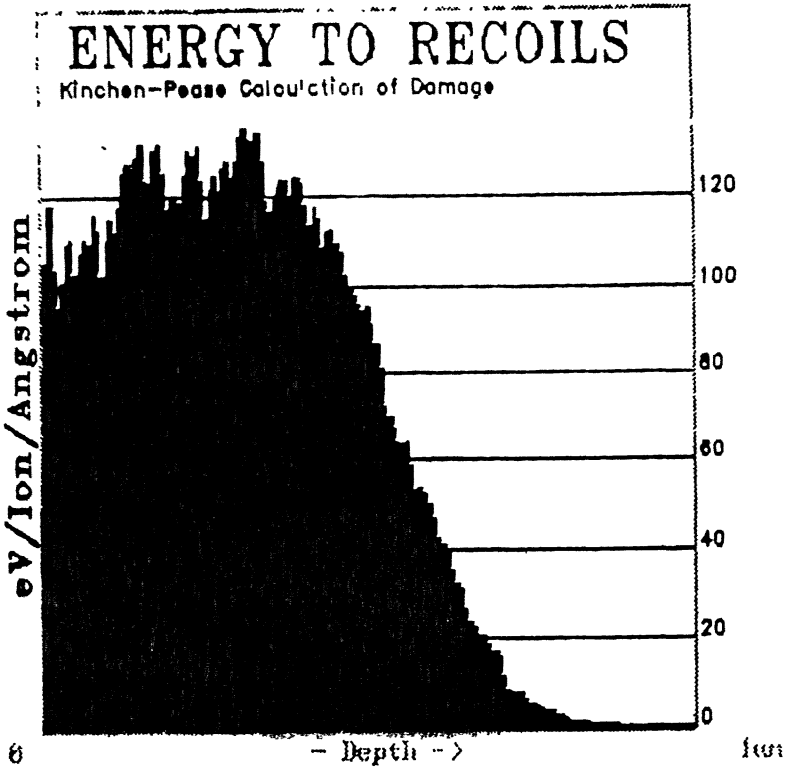

Fig. 2.2(a) TRIM calculations to estimate the total thickness of the sample. The fig. shows the energy deposited by the incident ion in the target.

TRIM 92

ION TYPE	Kr^+
ION ENERGY	1 MeV
ION ANGLE	0 Deg.

Target layers	Depth
$Si_{.5}Ge_{.5}$	1 μm

IONS COMPLETED 3000

	Range (A)
Longitudnal	4795
Lateral Projection	1023
Radial Projection	1599

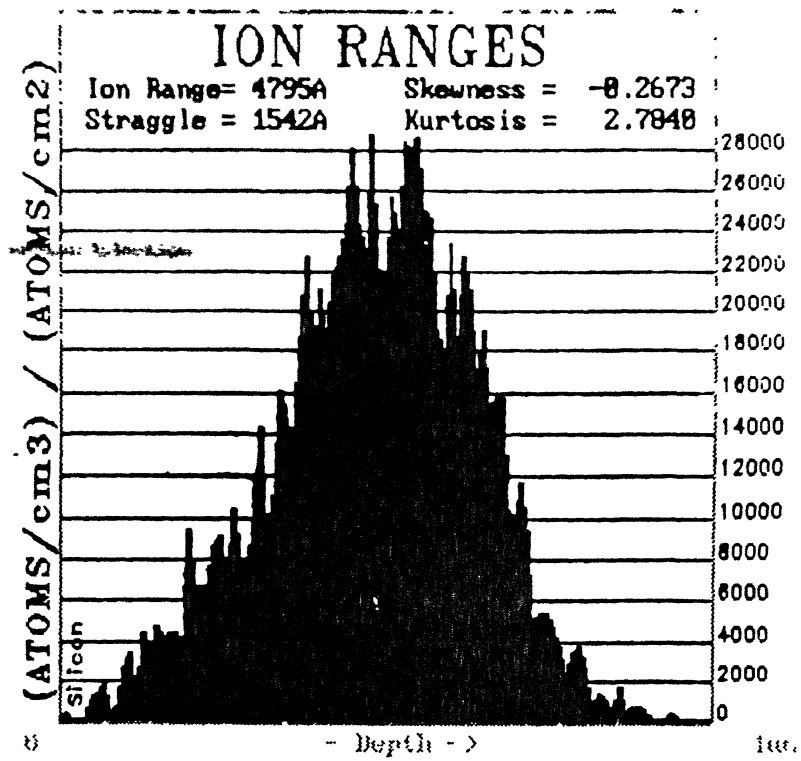

Fig. 2.2(b) TRIM calculations showing the range of Krypton ions in the substrate.

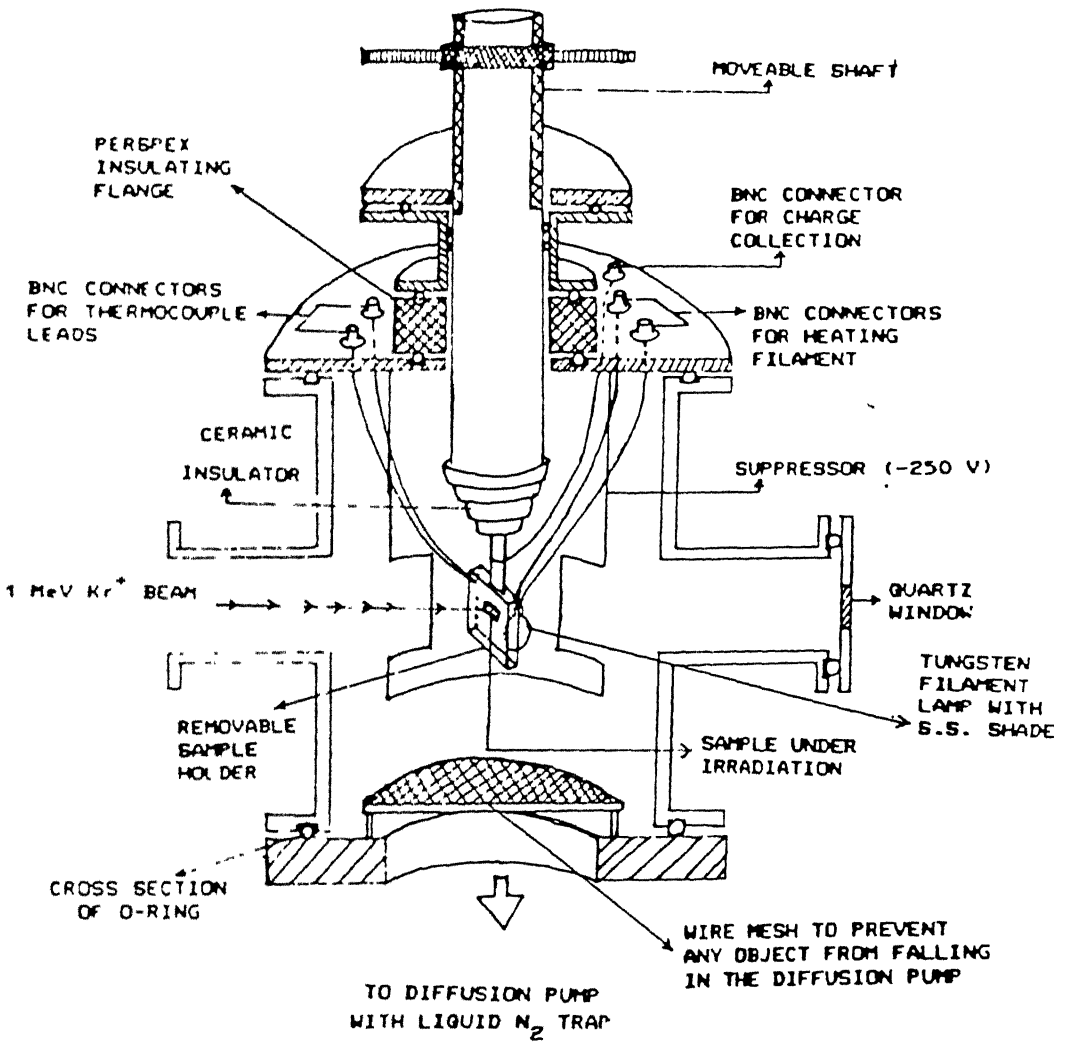

Fig. 2.3 The Heavy Ion Irradiation Chamber

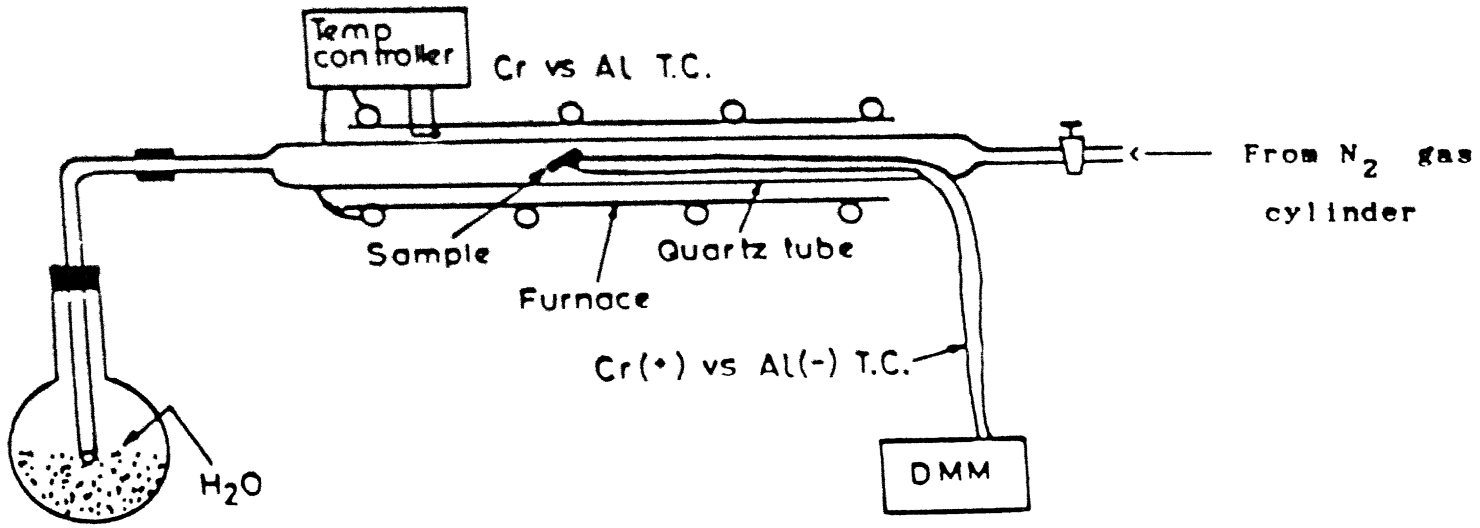

Fig. 2.4 Experimental arrangement for annealing the samples

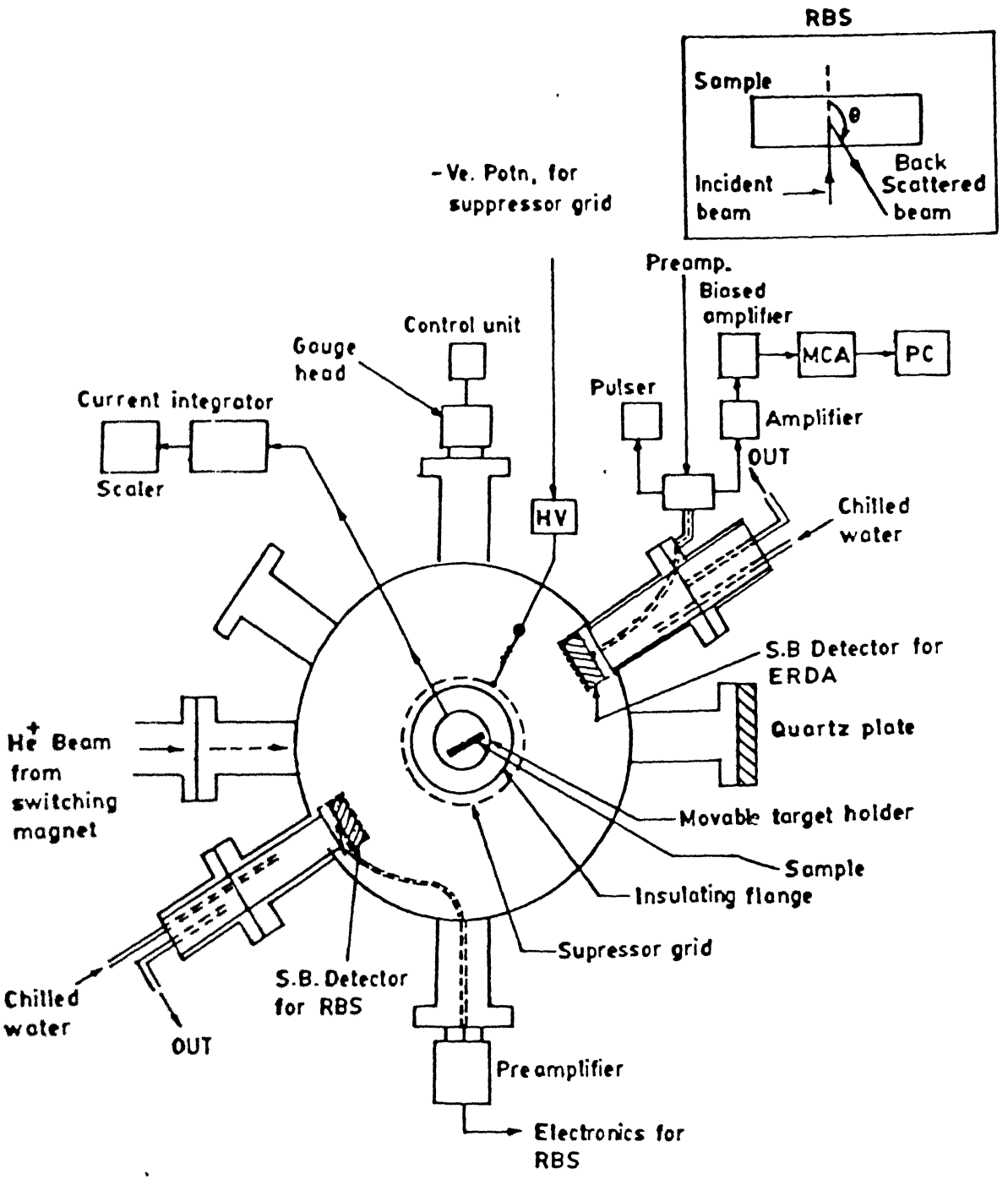

Fig. 2.5 The RBS Chamber

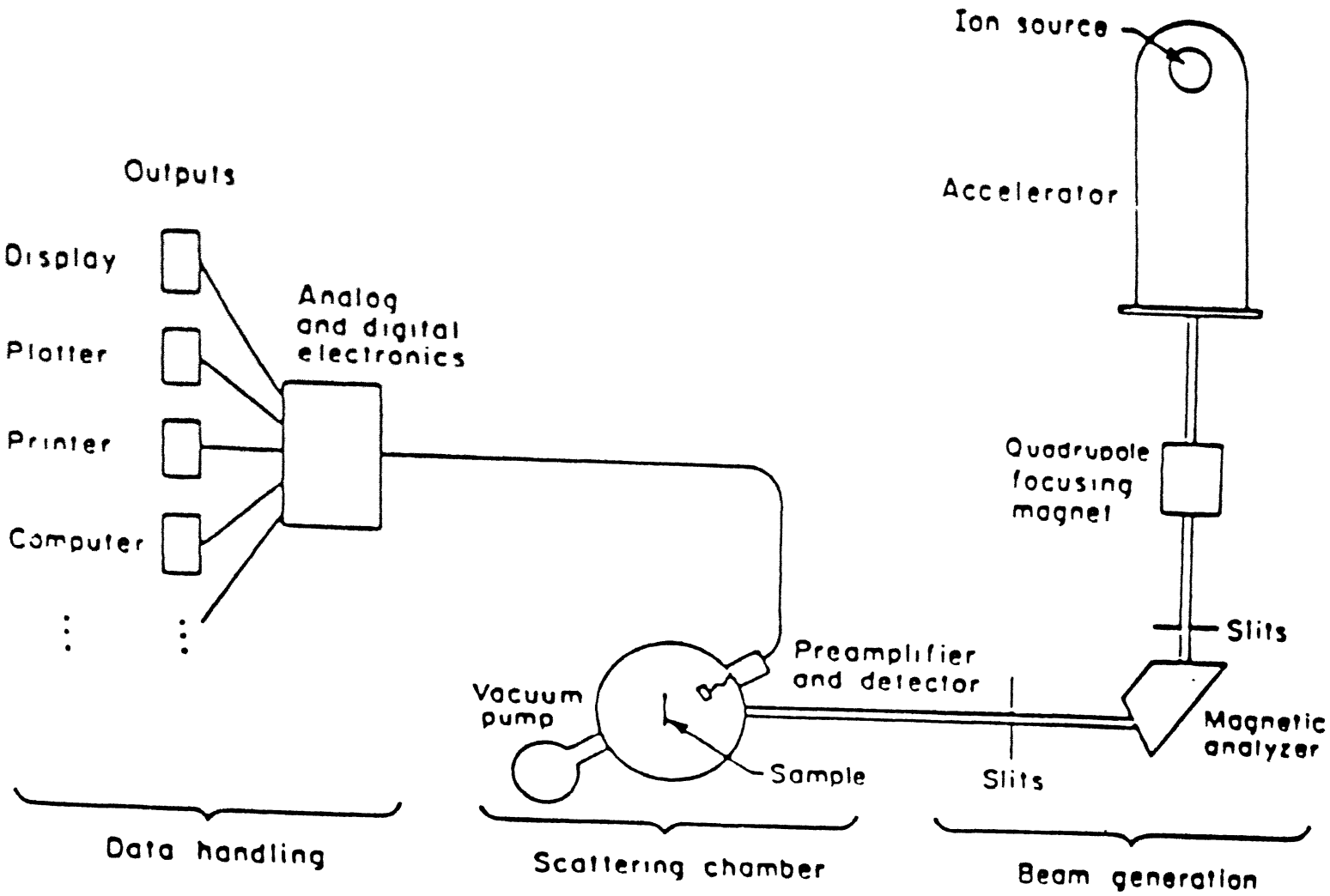

Fig. 2.6 Schematic diagram of a typical backscattering spectrometry system in use today.

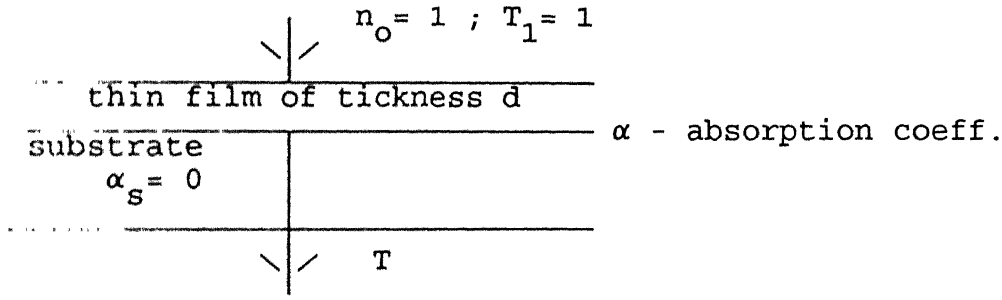

Fig 2.7

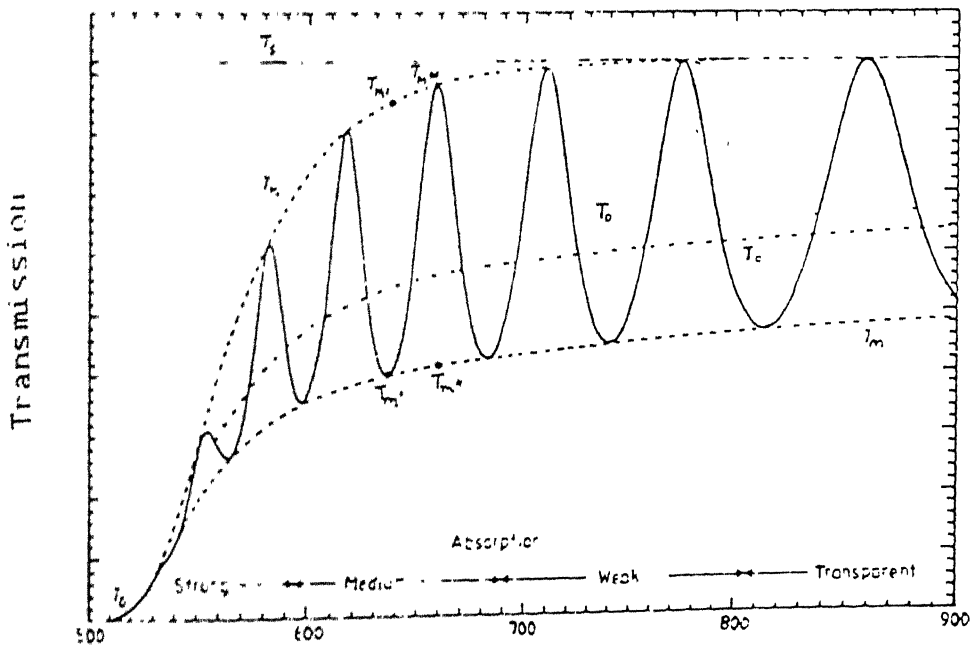

Fig. 2.8 Typical Transmission Spectra obtained

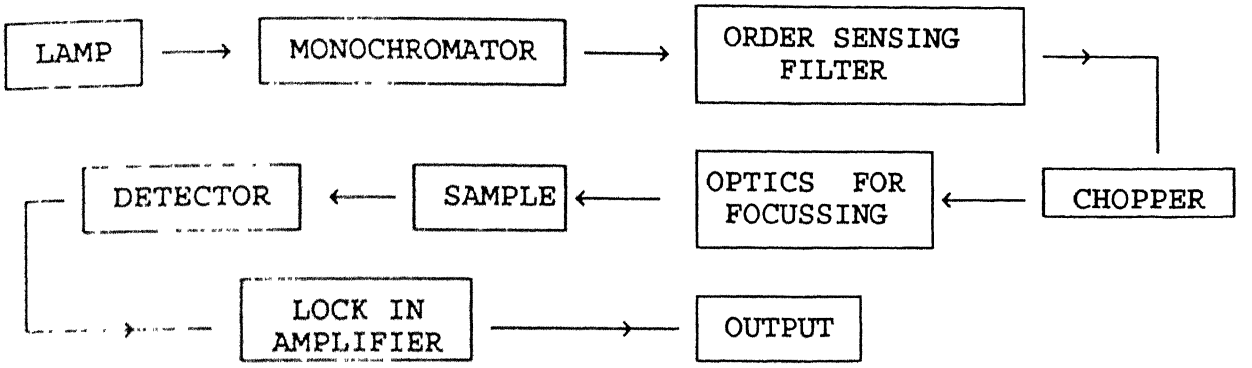

Fig 2.9

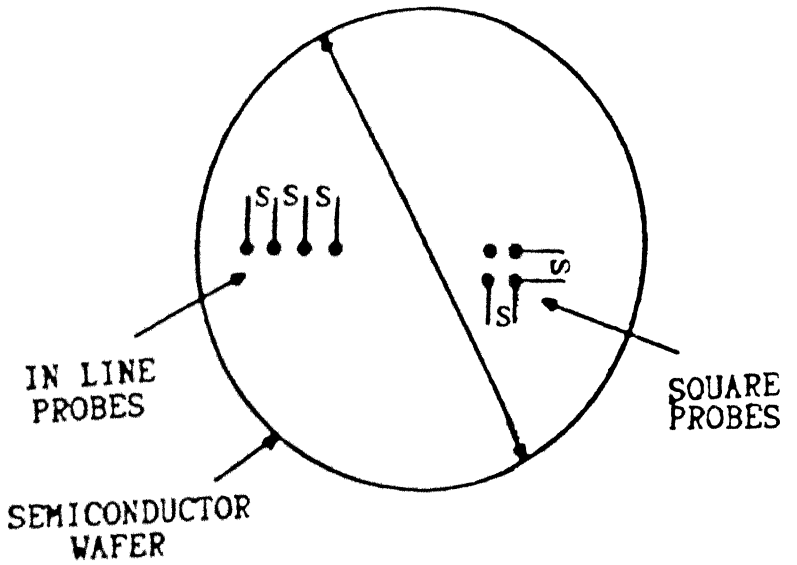

Fig. 2.11 The layout of 'in-line' and 'square' four point probe geometries. 'S' is the probe spacing.

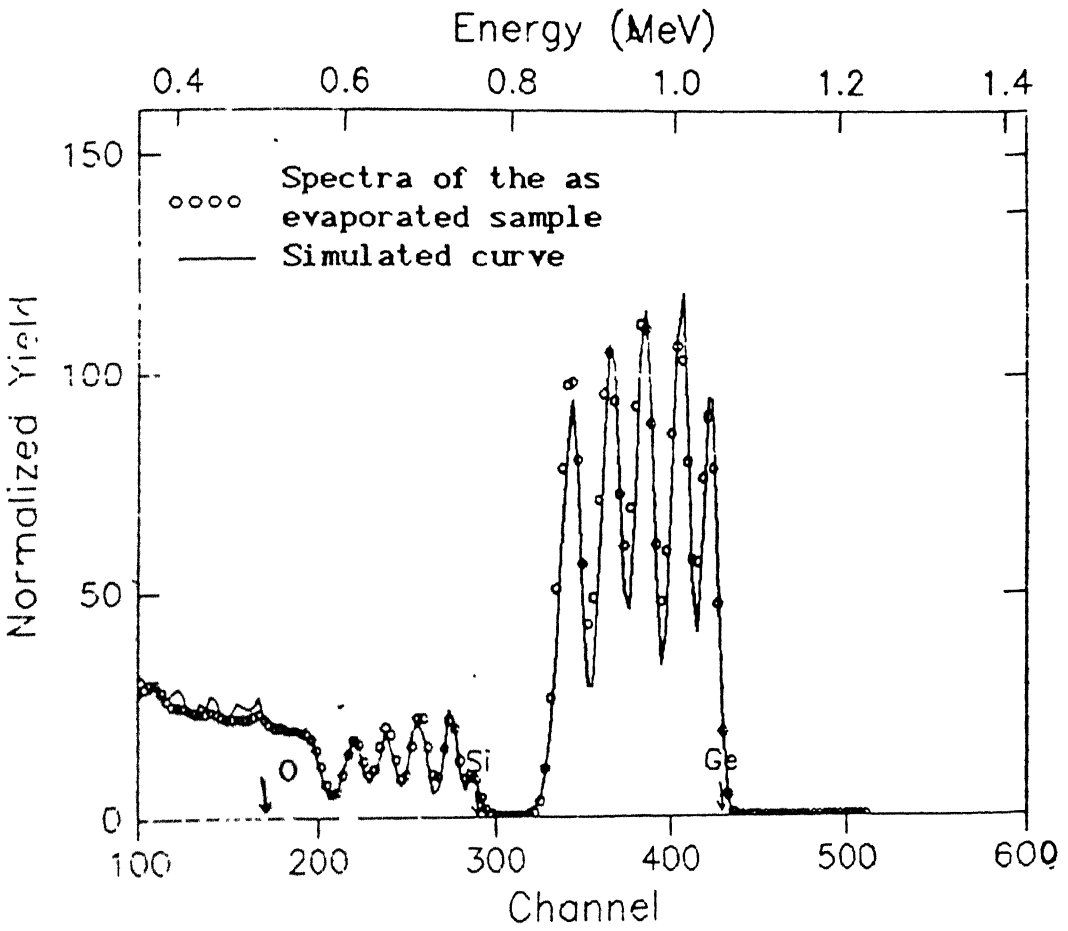

Fig. 3.1 RBS spectra of the as evaporated sample along with the simulated curve (10 layers)

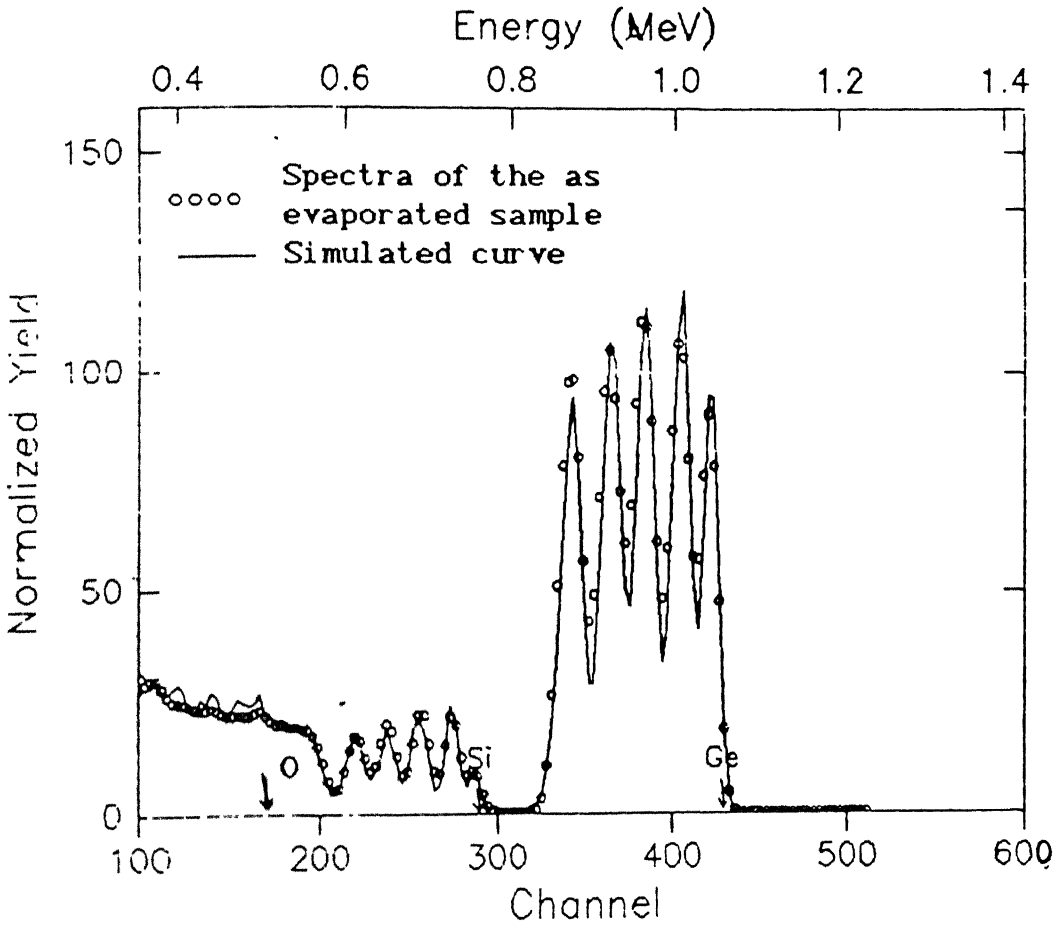

Fig. 3.1 RBS spectra of the as evaporated sample along with the simulated curve (10 layers)

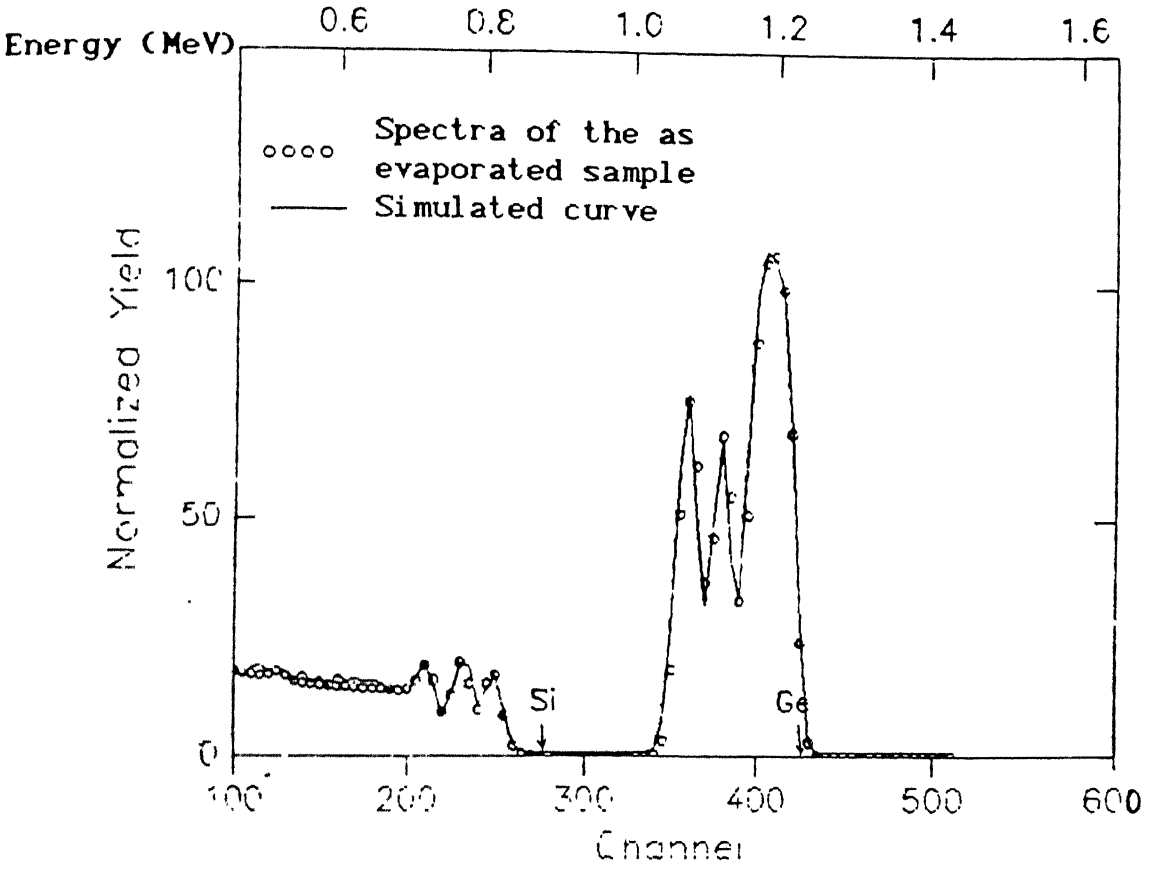

Fig. 3.2 RBS spectra of the as evaporated sample along with the simulated curve (6 - layer)

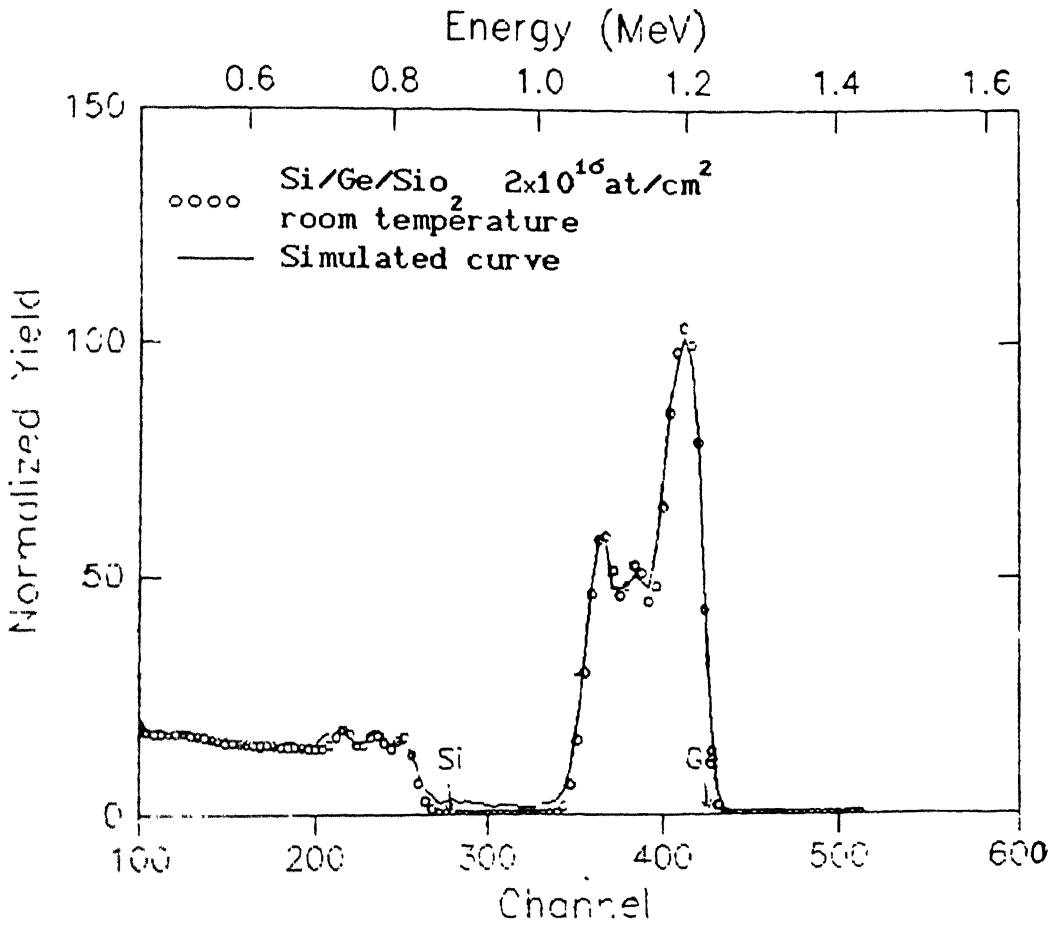

Fig. 3.4 RBS spectra for the sample irradiated with a dose of 2×10^{16} at/cm^2 at room temperature with the simulated curve

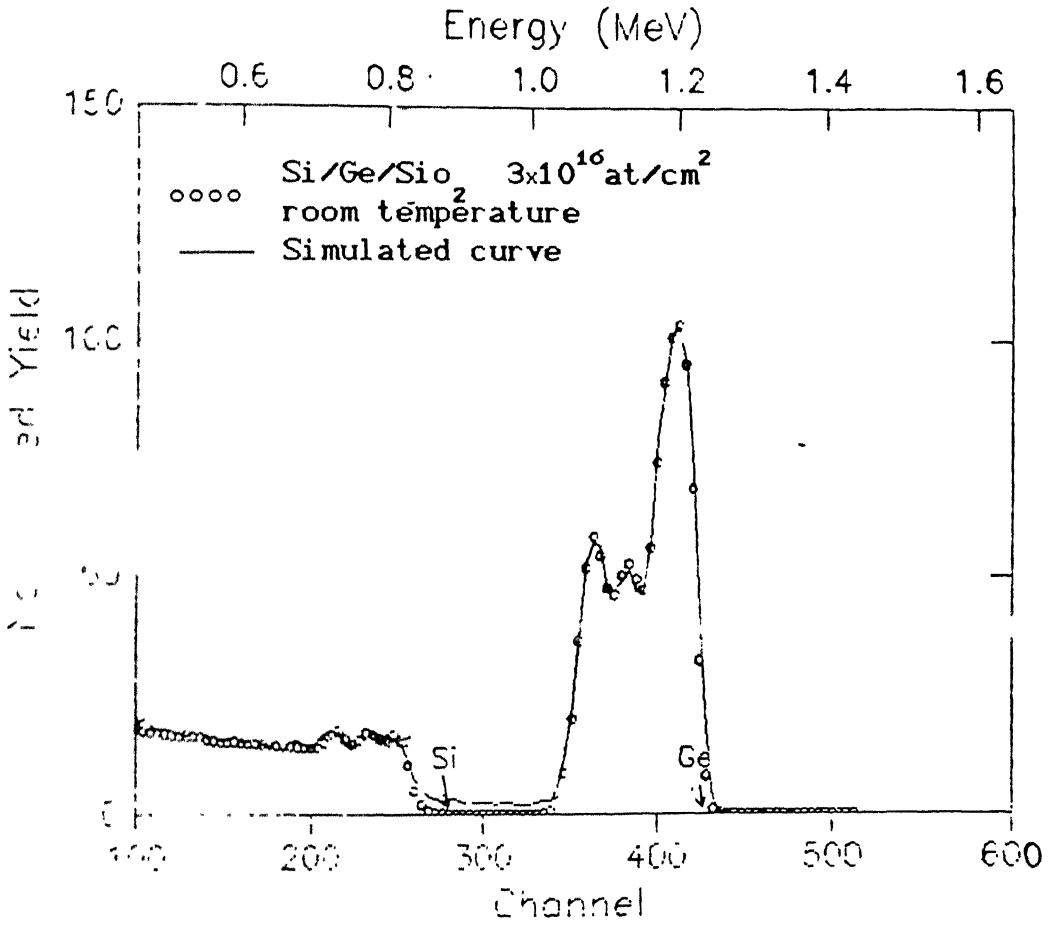

Fig. 3.5 RBS spectra for the sample irradiated with a dose of 3×10^{16} at/cm^2 at room temperature with the simulated curve

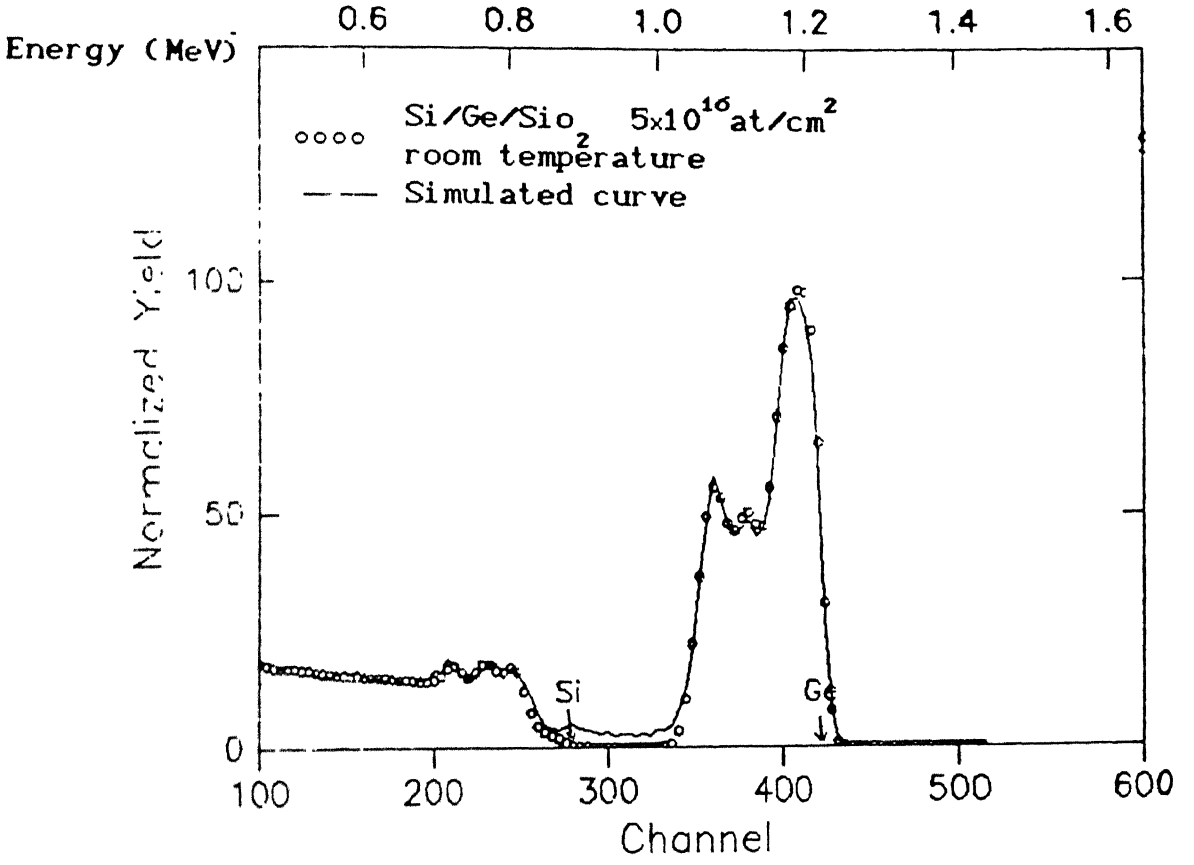

Fig. 3.6 RBS spectra for the sample irradiated with a dose of 5×10^{16} at/cm^2 at room temperature with the simulated curve

TRIM 92

ION TYPE Kr^+
ION ENERGY 1 MeV
ION ANGLE 0 Deg.

Target layers Depth

Si & Ge layers of total thickness 2700 A on SiO_2 Substrate

IONS COMPLETED 3000

	Range (A)
Longitudnal	6365
Lateral Projection	1402
Radial Projection	2217

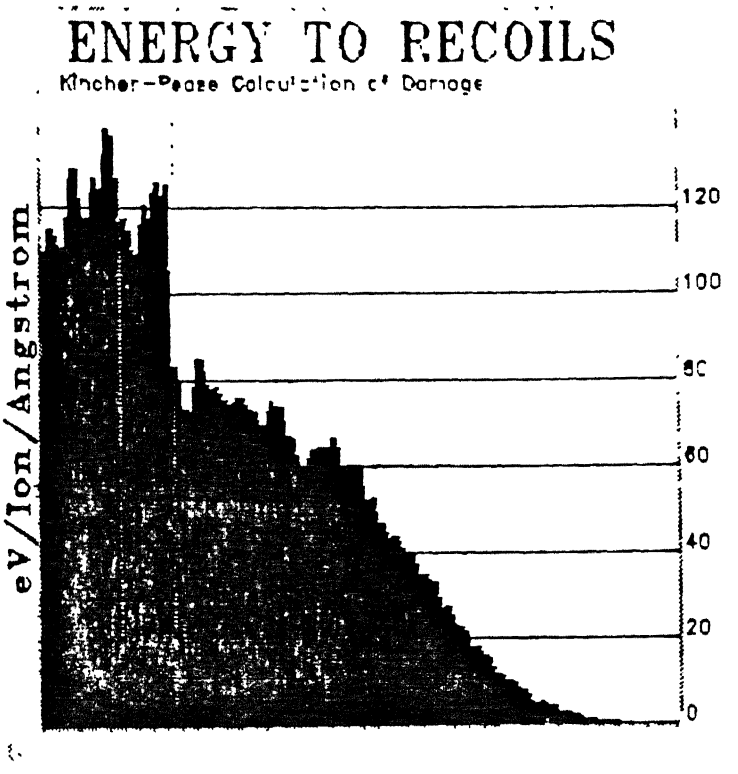

Fig. 3.7 TRIM calculations for the 6 layered samples showing the energy deposited by the incident ion

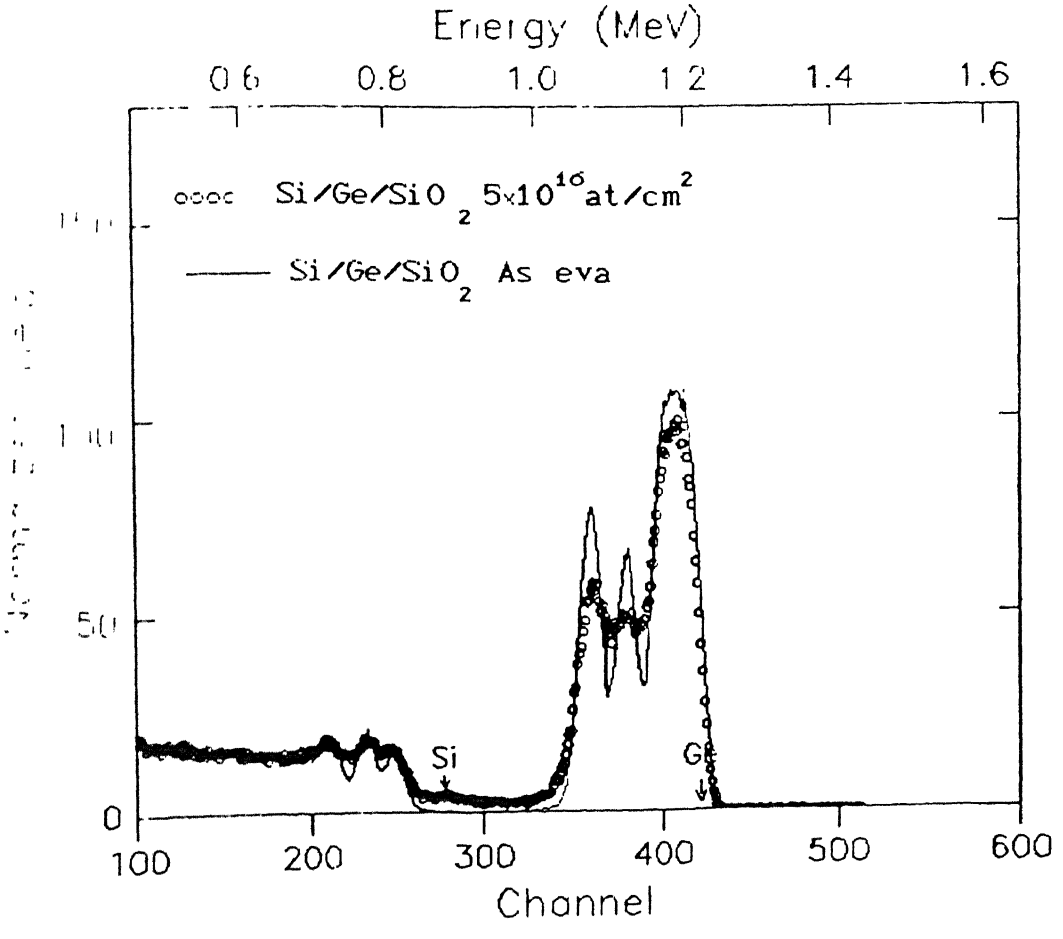

Fig. 3.8 Comparison of the RBS spectra to illustrate the progress in mixing with varying irradiating condition

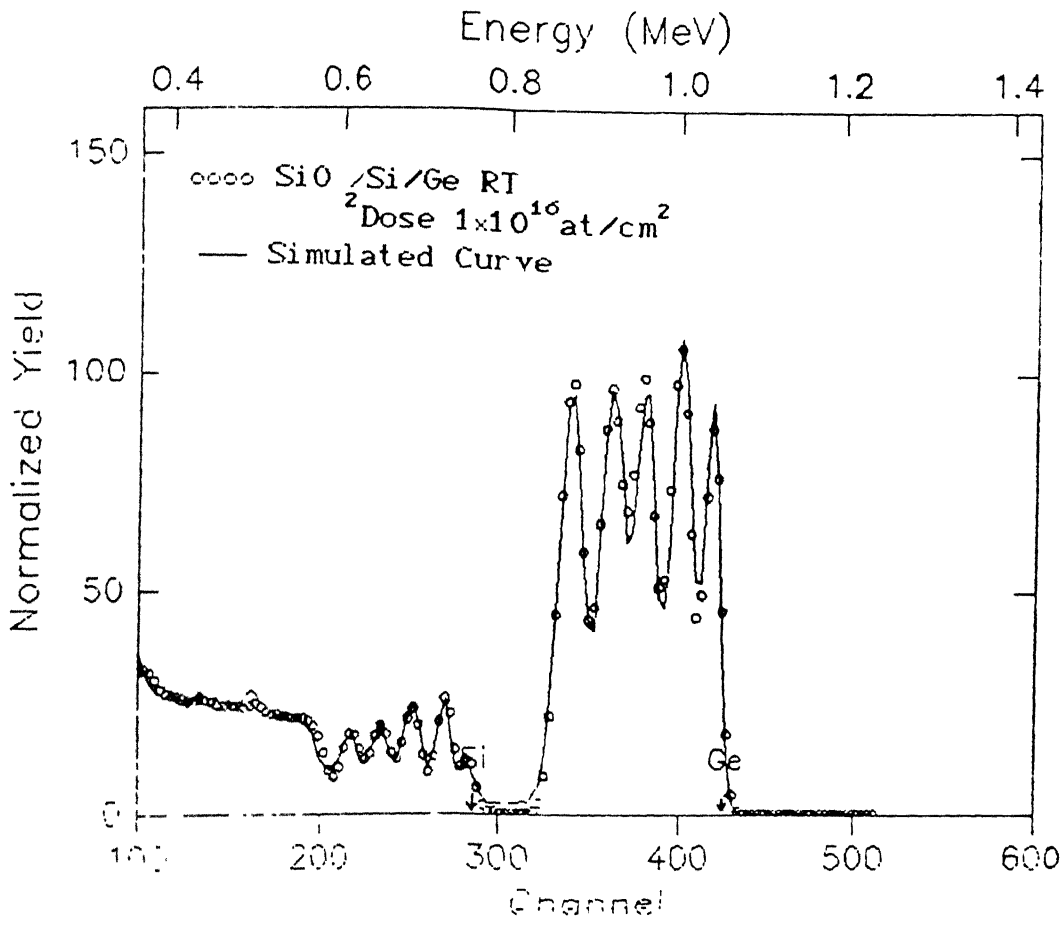

Fig. 3.10 RBS spectra for the sample irradiated with a dose of 1×10^{16} at/cm^2 at room temperature

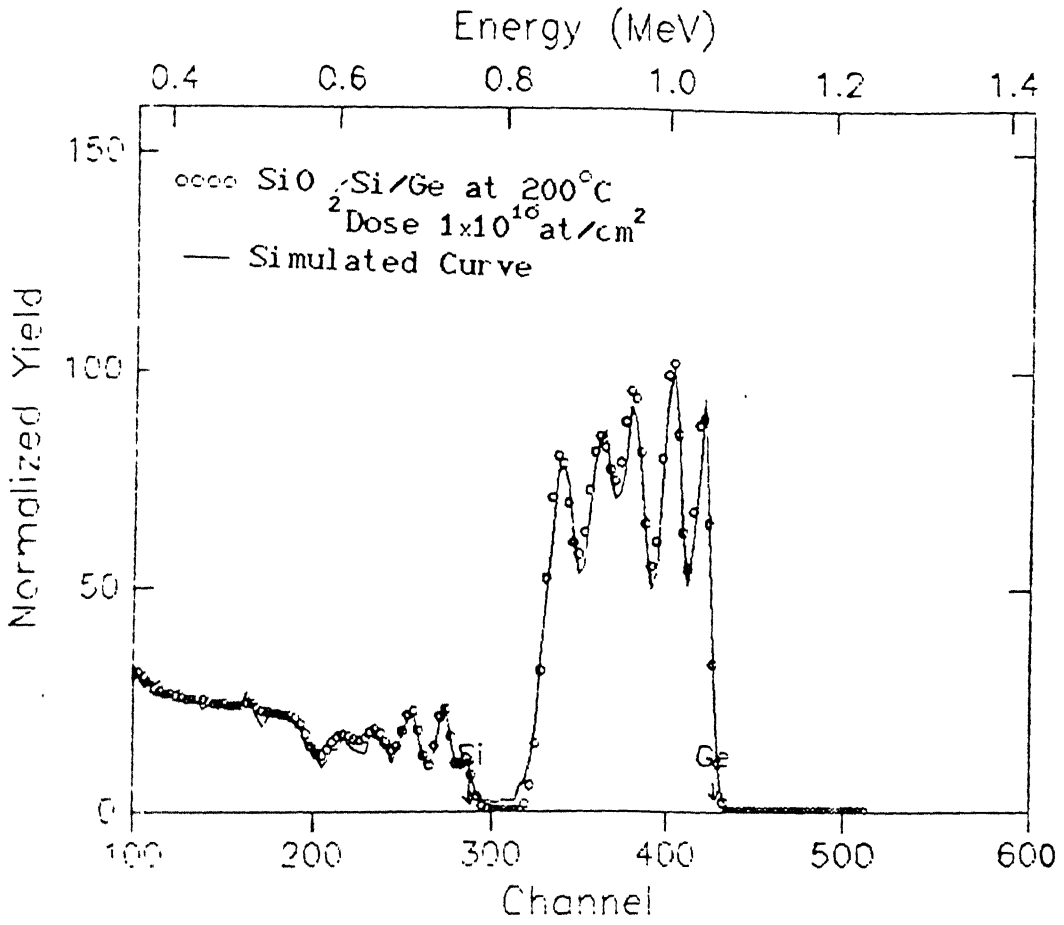

Fig. 3.11 RBS spectra for the sample irradiated with a dose of 1×10^{16} at/cm^2 at 200°C (High T)

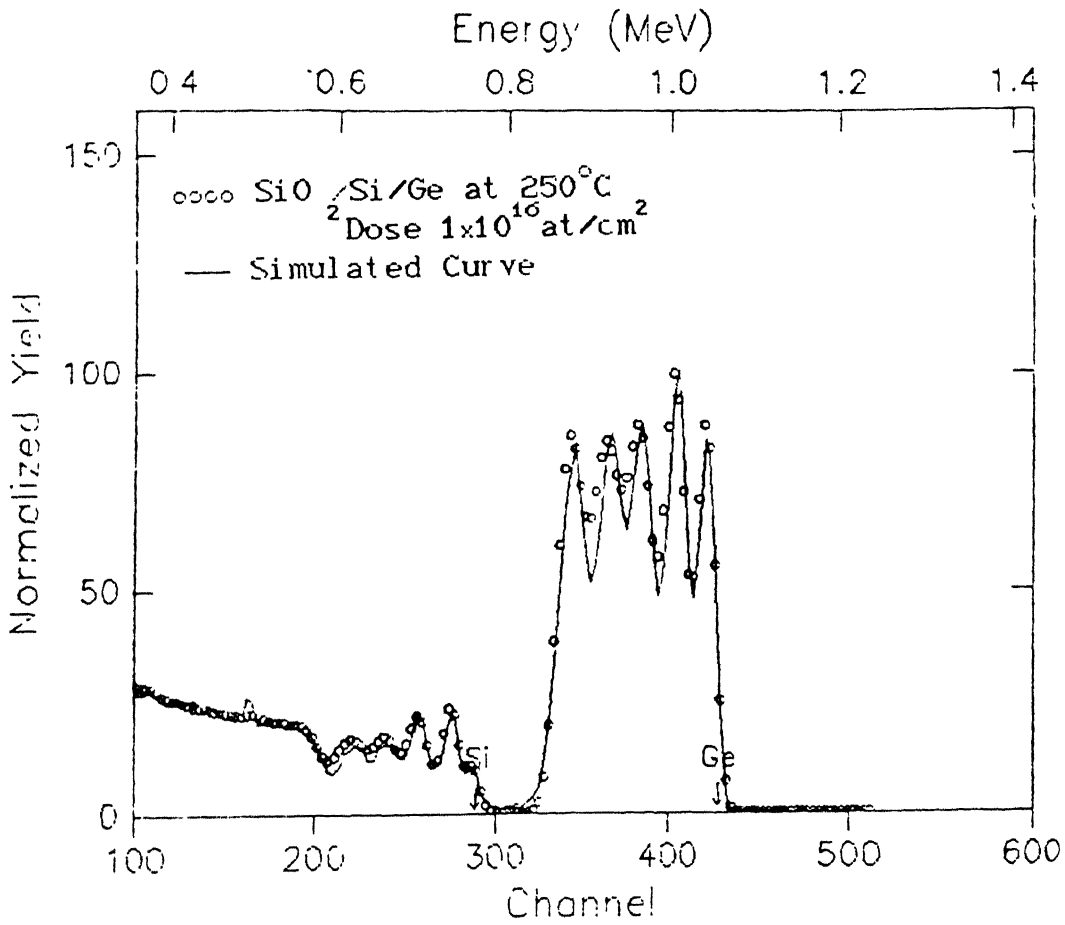

Fig. 3.12 RBS spectra for the sample irradiated with a dose of 1×10^{16} at/cm^2 at 250°C (High T)

TRIM 92

ION TYPE	Kr^+
ION ENERGY	1 MeV
ION ANGLE	0 Deg.

Target layers Depth

Si & Ge layers of total thickness 3200 A on SiO_2 Substrate

IONS COMPLETED 3000

	Range (A)
Longitudnal	6091
Lateral Projection	1345
Radial Projection	2134

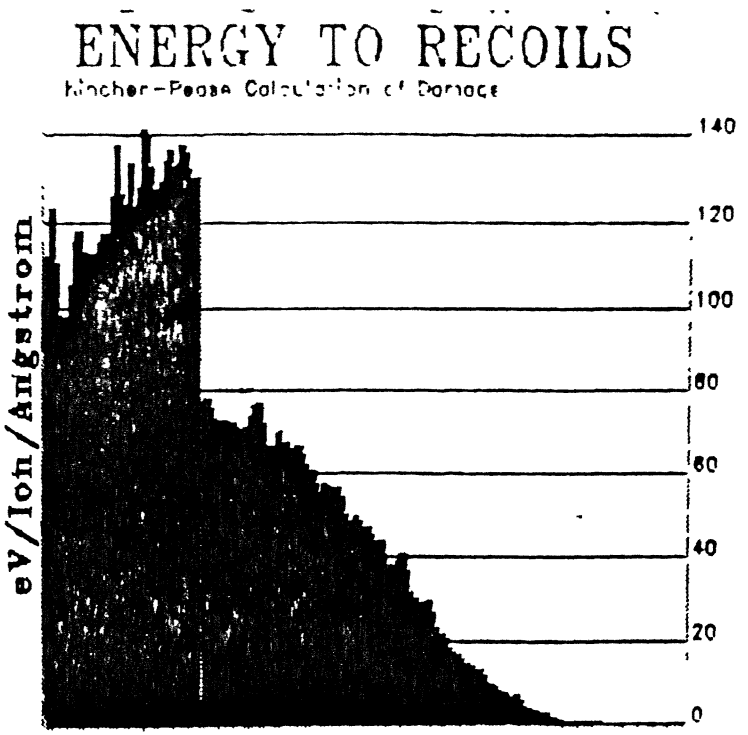

Fig. 3.13 TRIM calculations for the 10 layered samples showing the energy deposited by the incident ion

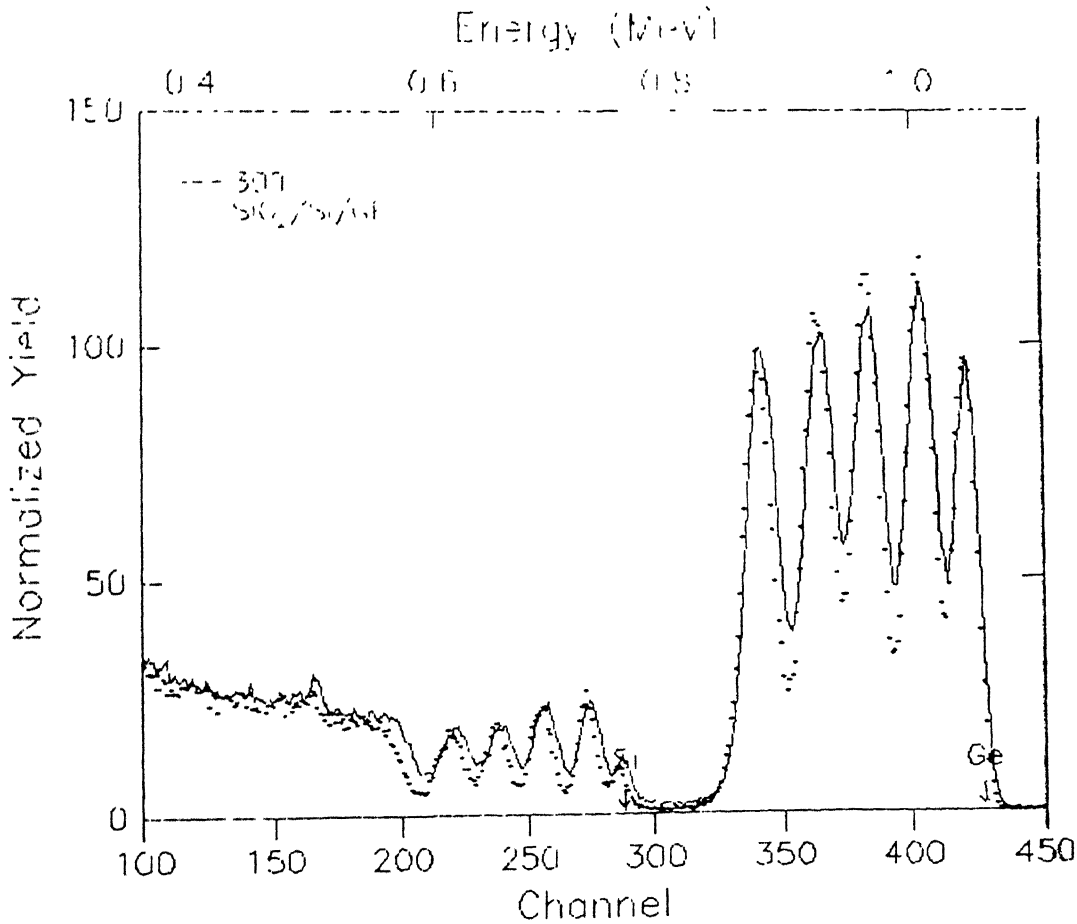

Fig .3.14 Comparison of the RBS spectra obtained from sample irradiated at 300°with the as evaporated sample

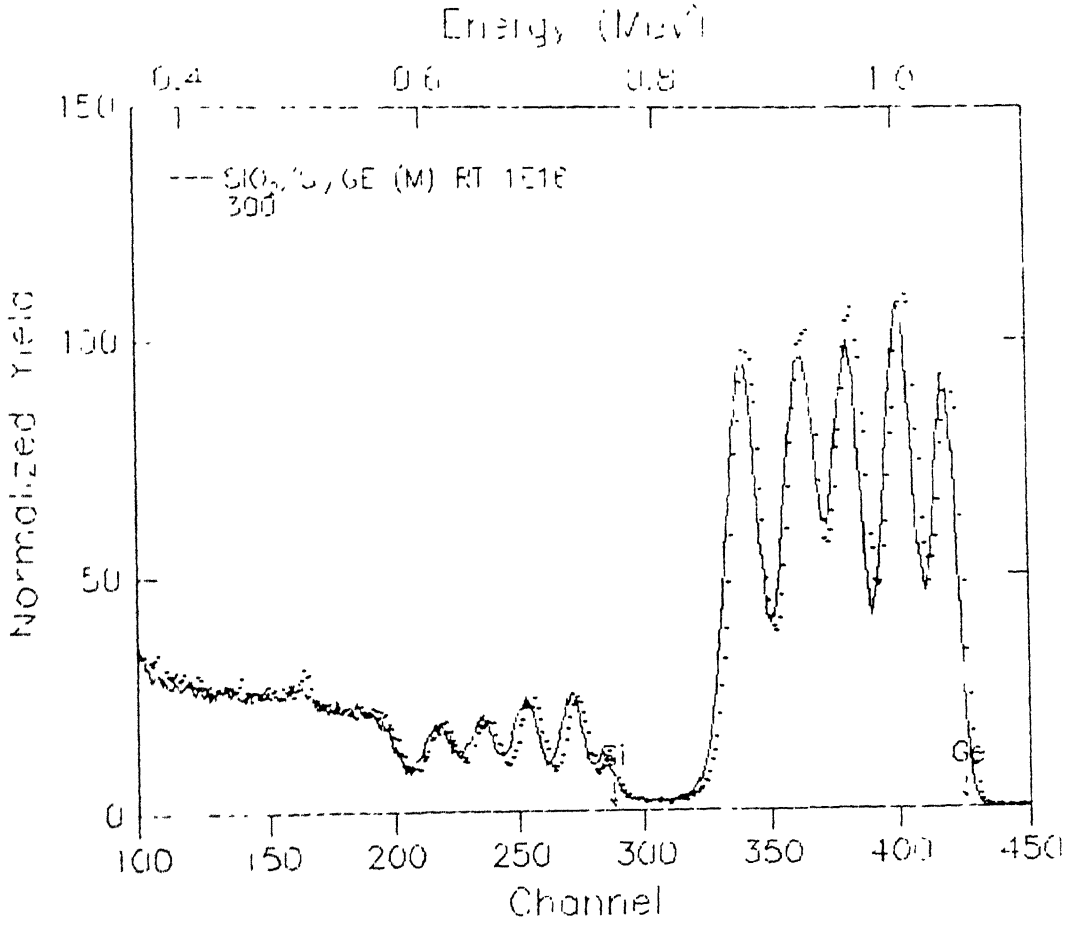

Fig .3.15 Comparison of the RBS spectra obtained from sample irradiated at 300°with the sample irradiated at room temperature

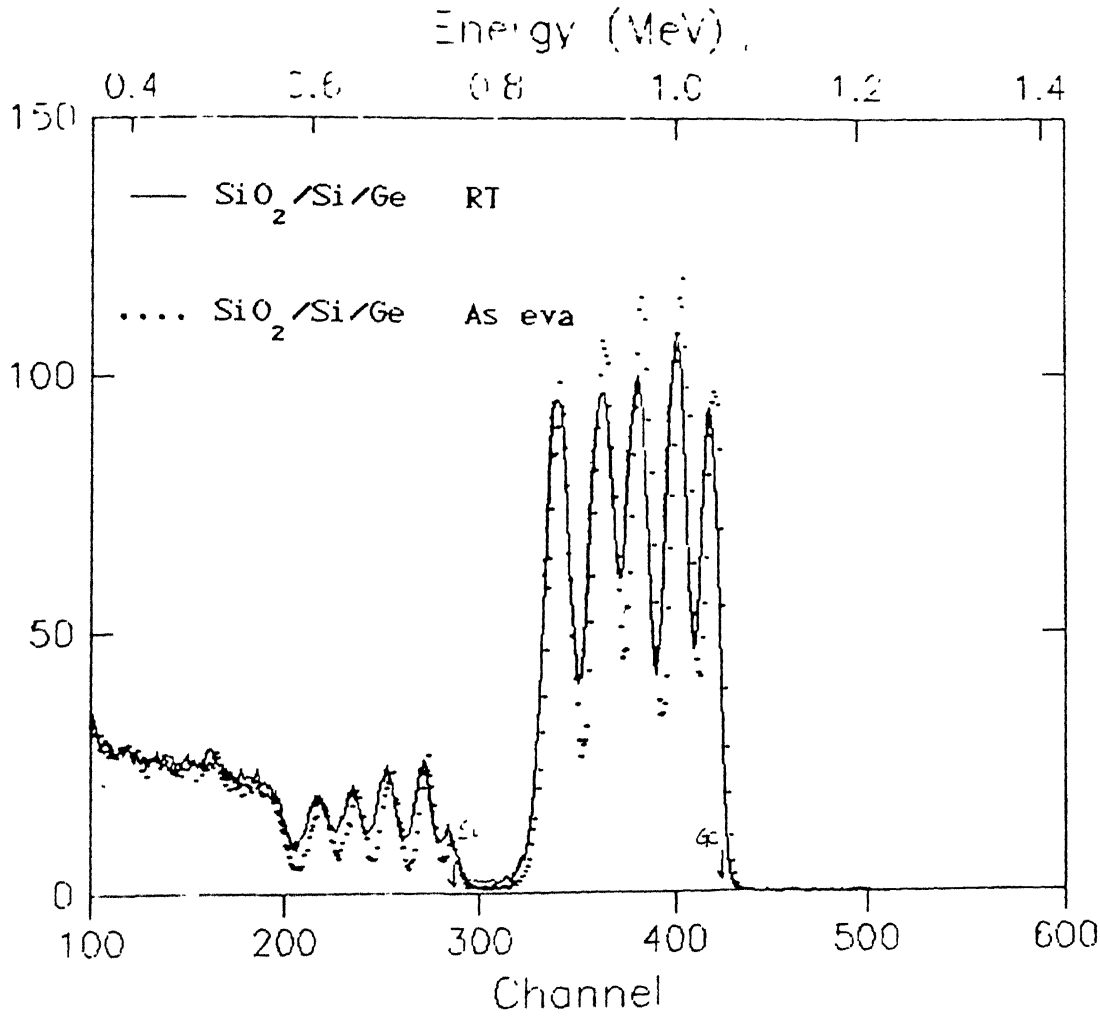

Fig. 3.16 Comparison of the RBS spectra to illustrate the progress in mixing with varying irradiation condition

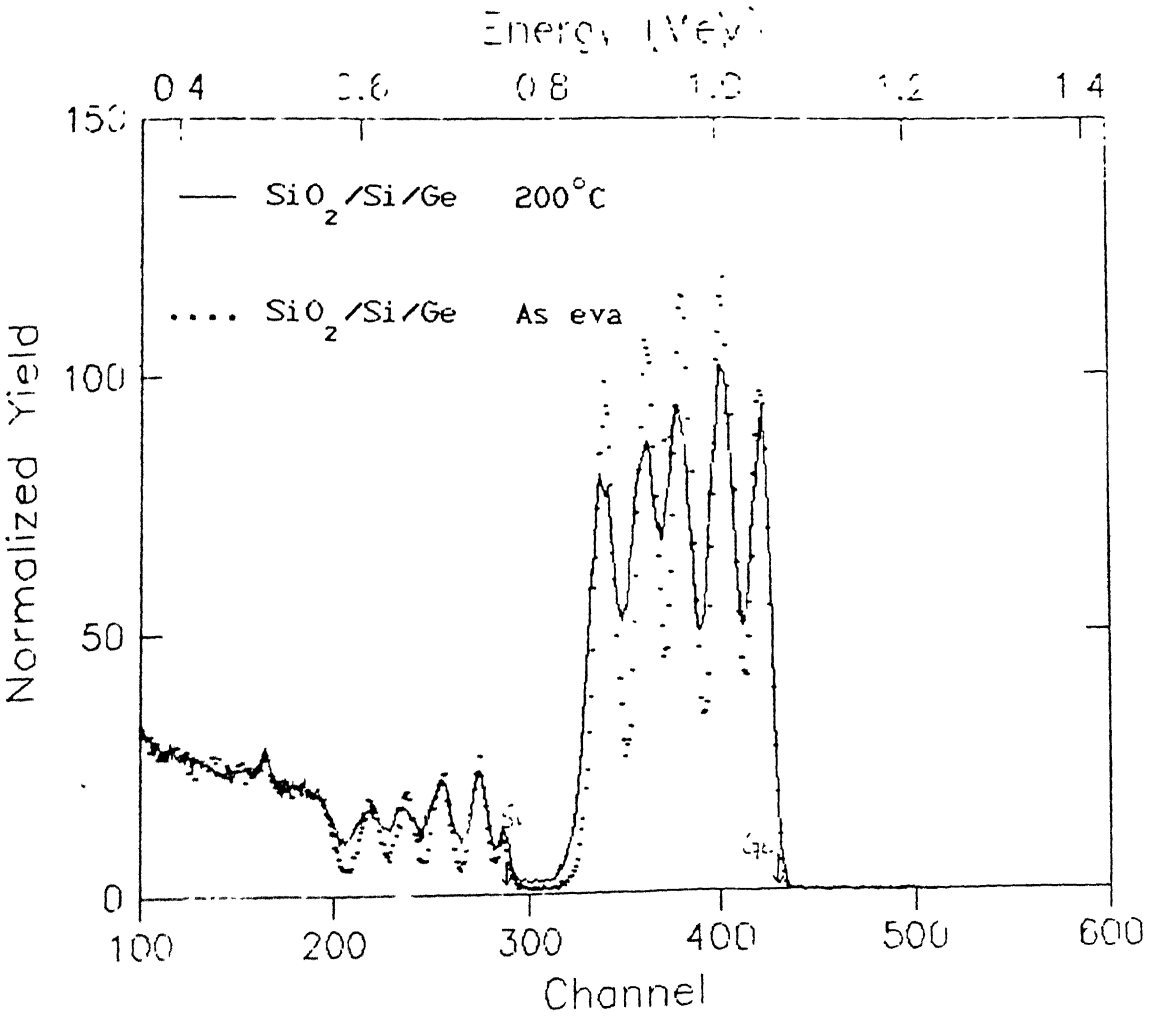

Fig. 3.17 Comparison of the RBS spectra to illustrate the progress in mixing with varying irradiation condition

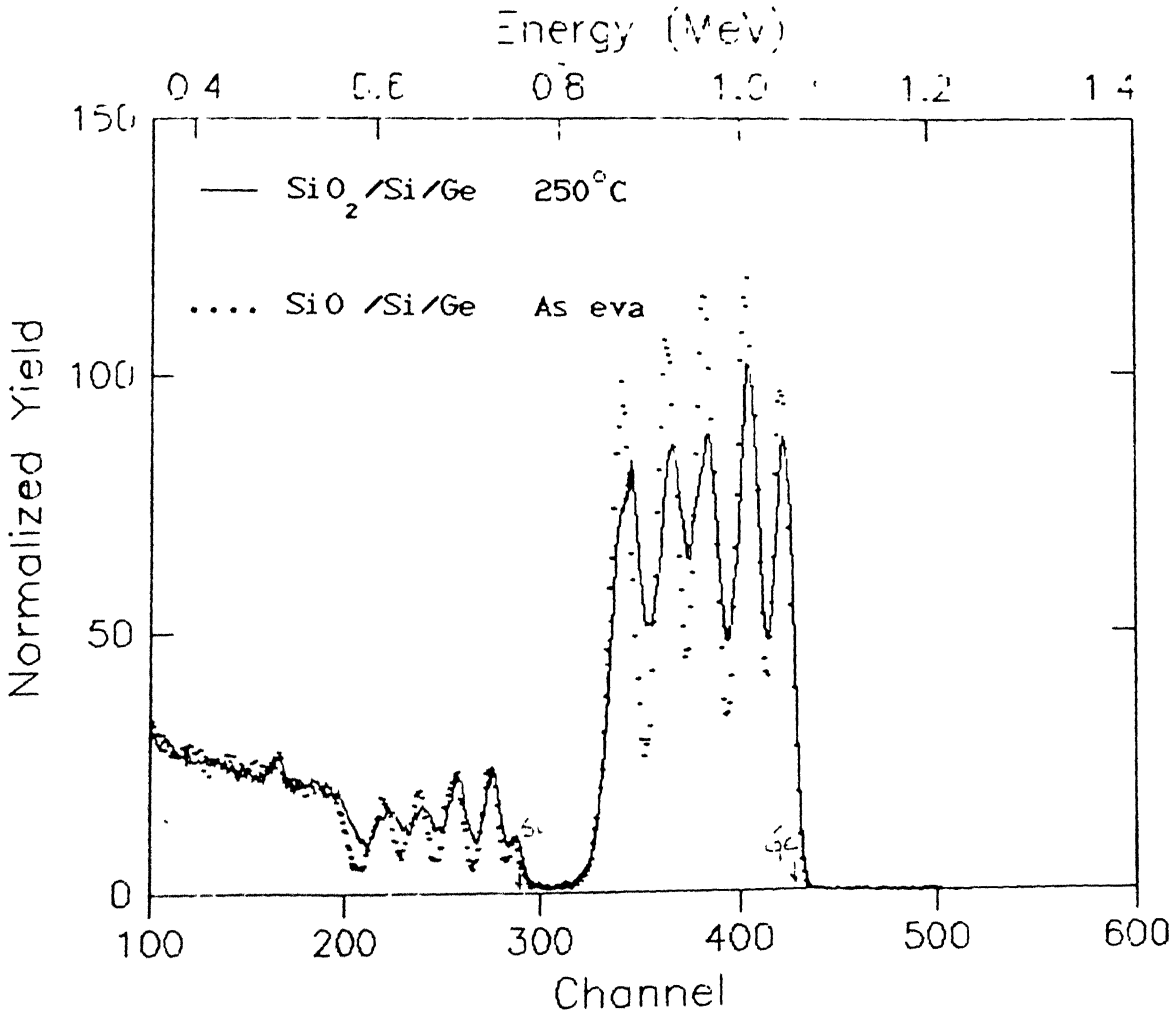

Fig. 3.18 Comparison of the RBS spectra to illustrate the progress in mixing with varying irradiating condition

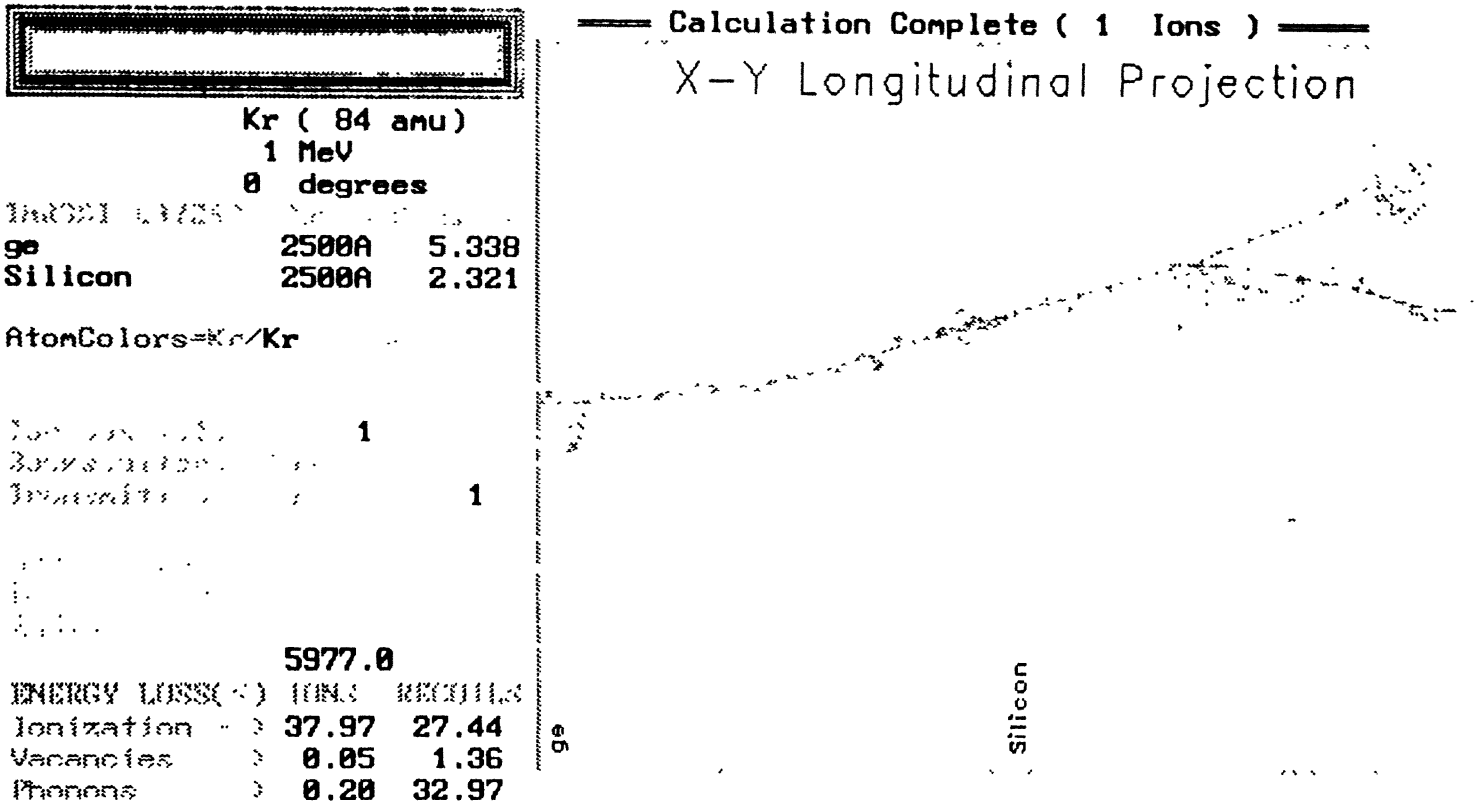

Fig. 3.19α TRIM calculations showing the cascade formation along with the ion trajectory for Si/Ge bilayer with Ge on top

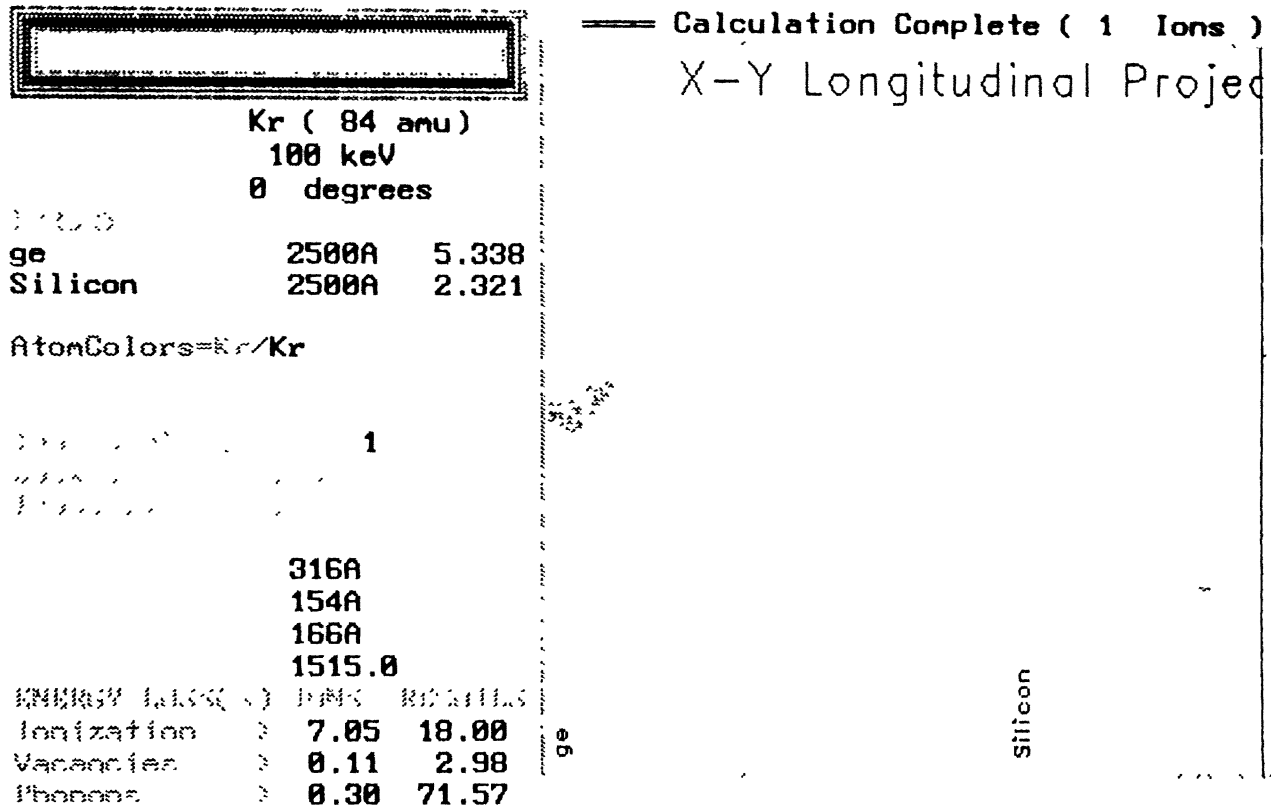

Fig. 3.19(b) TRIM calculations showing the cascade formation along with the ion trajectory for Si/Ge bilayer with Ge on top

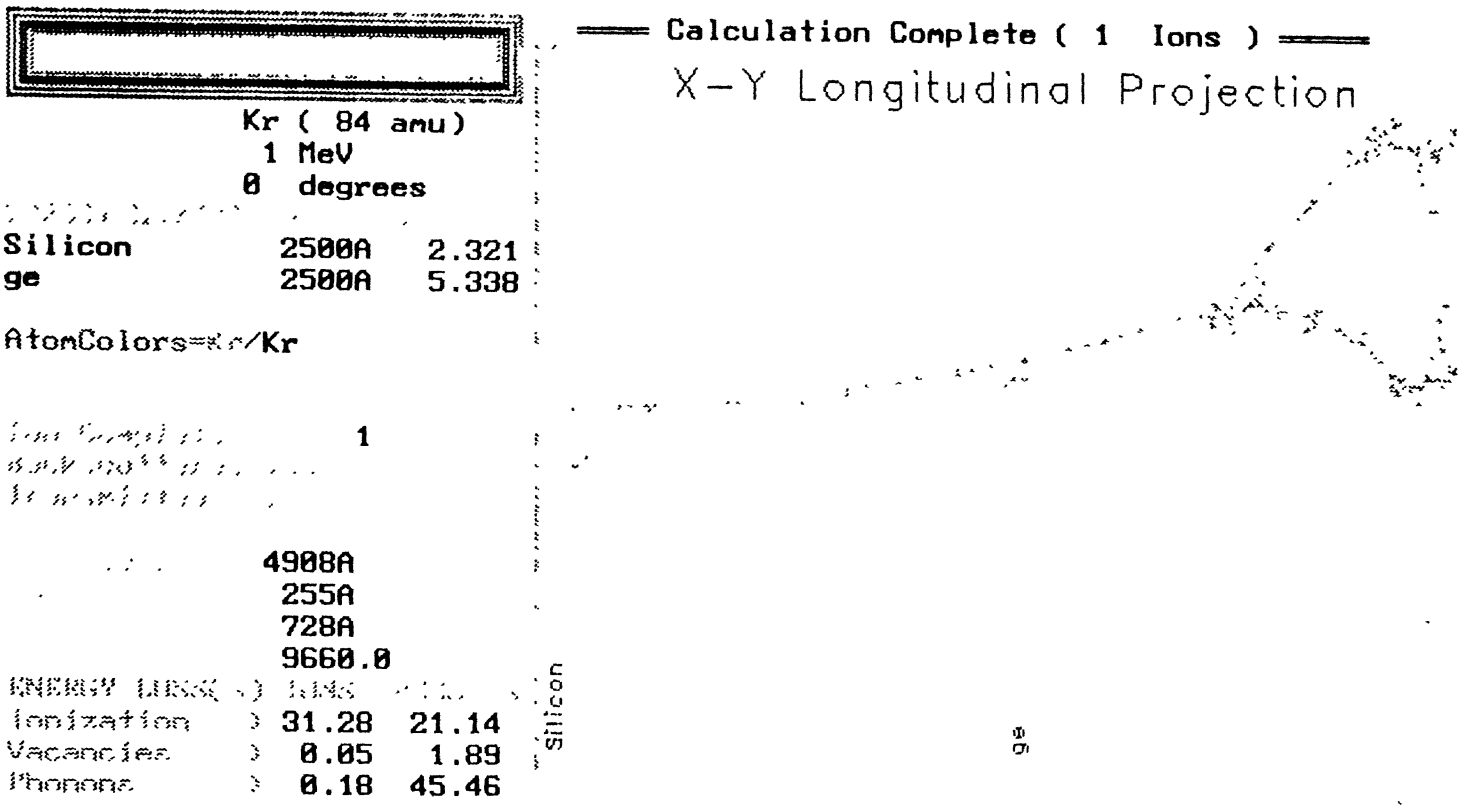

Fig. 3.20a TRIM calculations showing the cascade formation along with the ion trajectory for Si/Ge bilayer with Si on top

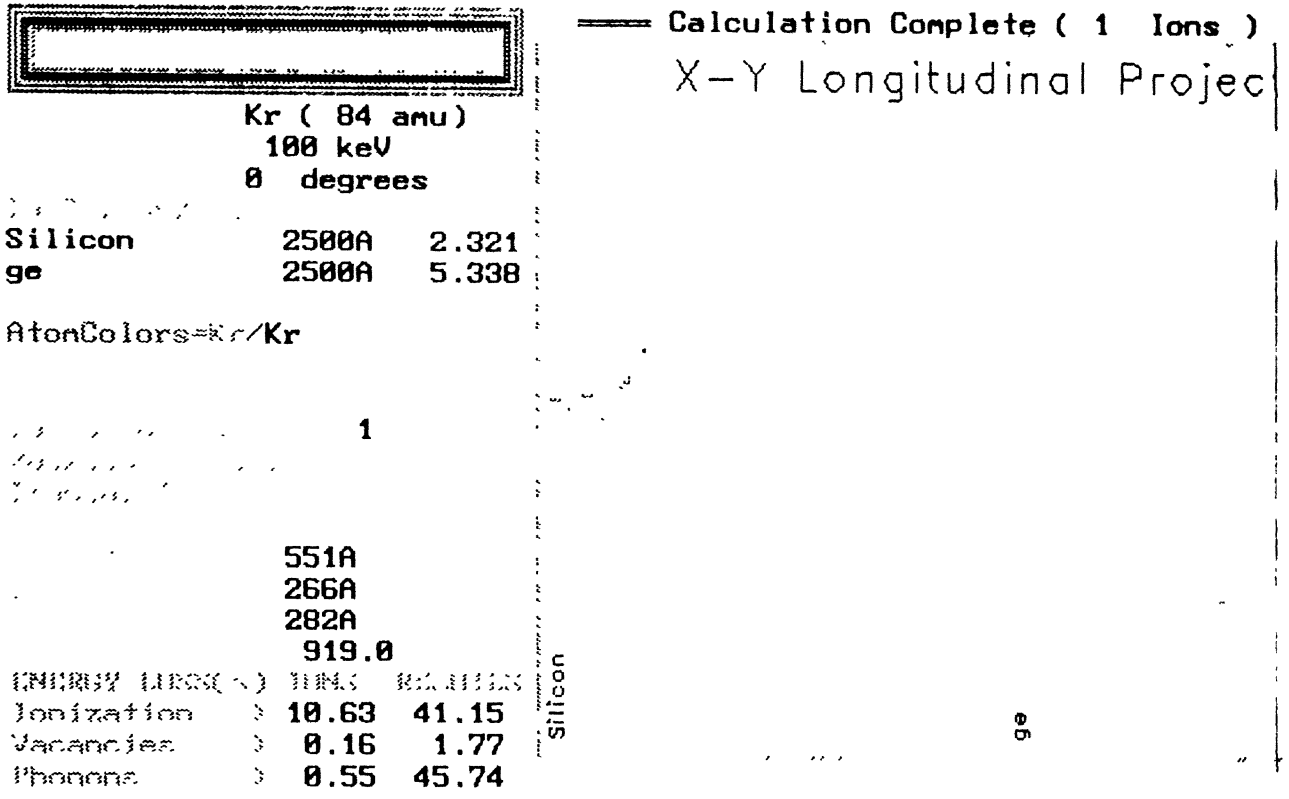

Fig. 3.20(b) TRIM calculations showing the cascade formation along with the ion trajectory for Si/Ge bilayer with Si on top

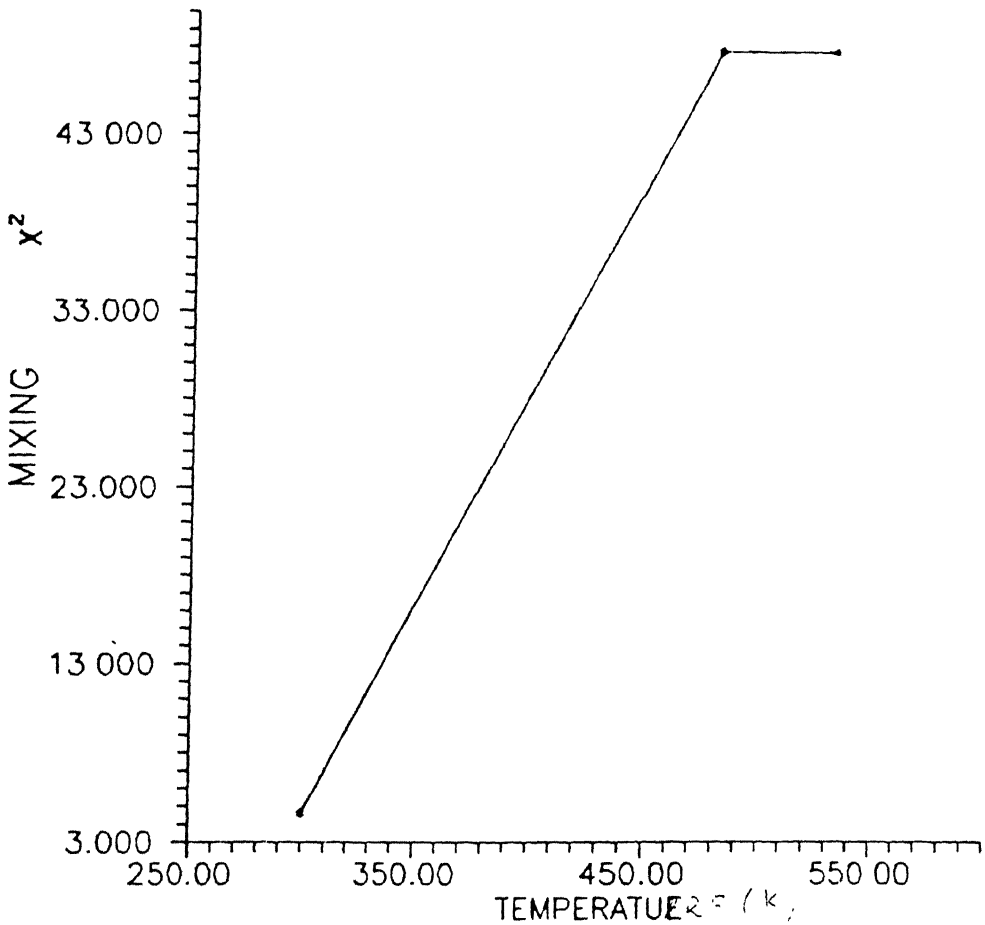

Fig. 3.21 Plot showing variation of the total mixed thickness with temperature

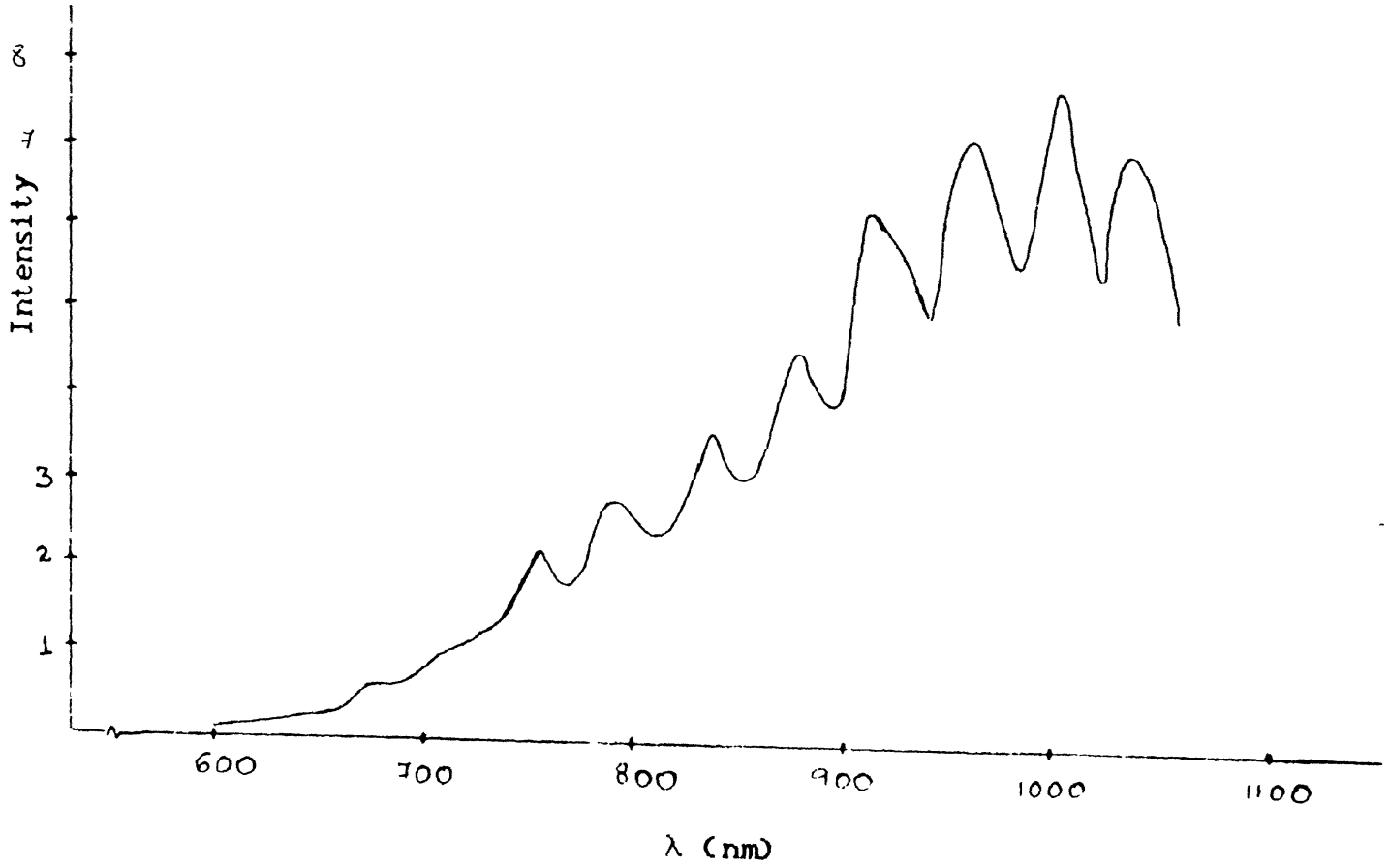

Fig. 3.22 Transmission spectra obtained during optical characterization of the samples (for sample irradiated at 200°C)

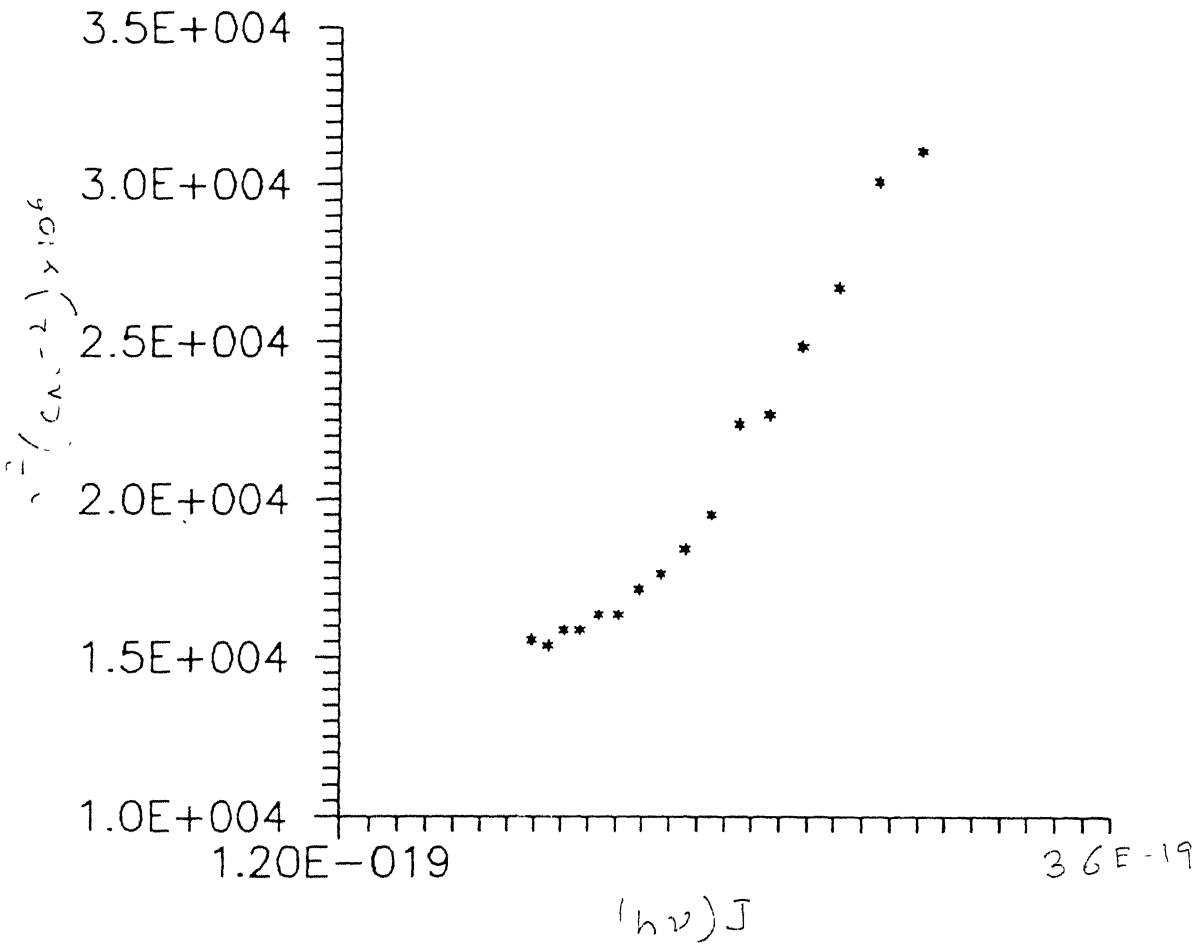

Fig. 3.23 Plot of α^2 vs (hν)

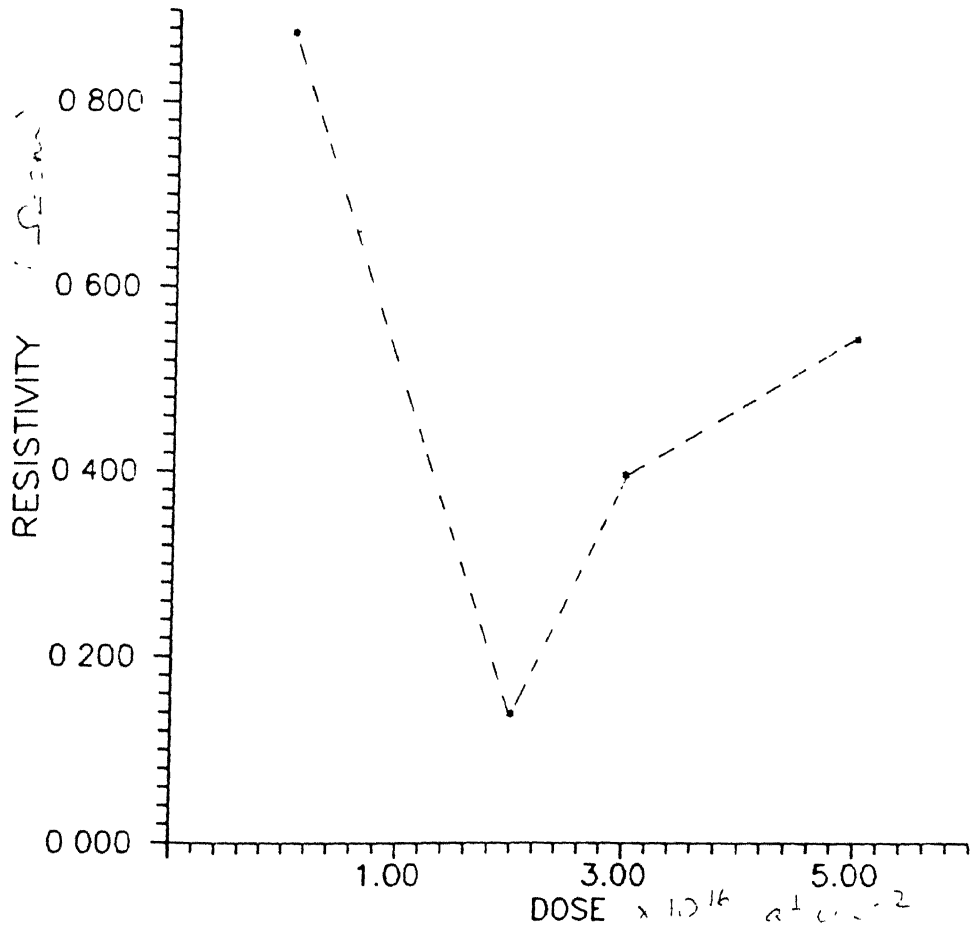

Fig. 3.24 Plot showing the variation of resistivity with dose

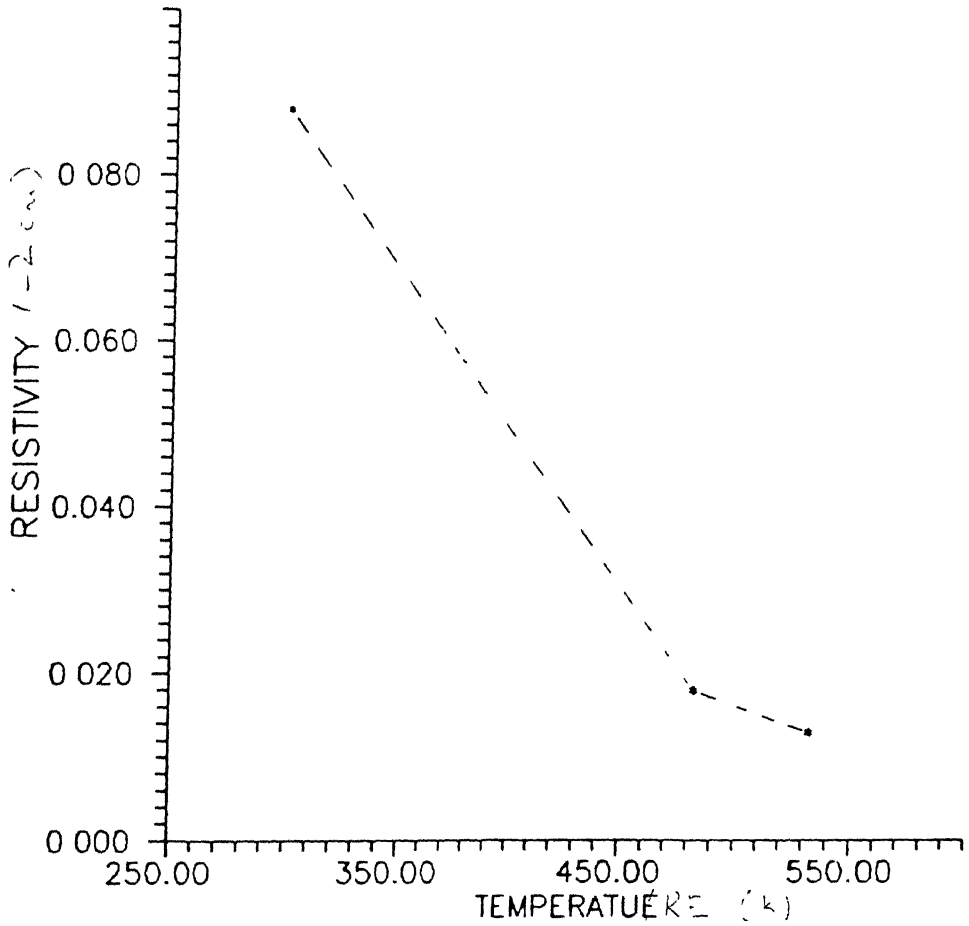

Fig. 3.25 Plot showing the variation of resistivity with substrate temperature during irradiation

REFERENCES

[1] Dearnaley G., J.H. Freeman, R.S. Nelson & J. Stephen in "Ion Implantation", North Holland Publishing Company, Amsterdam 1976.

[2] "Surface Alloying by Ions, Electrons and Laser Beams" (American Society for metals), ed. L.E. Rehn.

[3] Hiroven J.K., Proceedings of conference on The applications of Ion plating and Implantation to Materials (1985)

[4] Liu B.X., Phys. Stat. Sol.(a) 94, 11 (1986) Review Article

[5] Matteson S., M.A. Nicolet, Ann. Rev. Mater. Sci. (1983)13 , 337-62

[6] Galliard J.P. in "Surface Engineering", ed. R. Kosowsky & S.C. Singhal, Boston (1984)

[7] Hohmuth K., B. Rauschenbach, Nucl. Instrum. Meth Phys Res. B46, 276-83 (1990)

[8] Rossum Van M., M.A. Nicolet & C.H. Wills, J. Appl. Phys. 56(4), 1032-35 1984

[9] Paine B.M. & R.S. Averback, Nucl. Instrum. Meth. Phys. Res. B7/8, 1985 666

[10] King W.E. & R. Benedeck, J. Nucl. Mater 117, 26 1983

[11] Guinan M.W. & J.H.Kinney, J. Nucl. Mater. 103/104, 1319 1981

[12] Johnson W.L. et al., Nucl. Instrum. Meth Phys. Res. B 7/8, 1985, 657

[13] Liu B.X., Nucl. Instrum. Meth. Phys. Res. B 7/8, 1985

[14] Xia W. et al, Appl. Phys. Lett. 55, (1989) 2020

[15] Xia W. et al, Nucl. Instrum. Meth. Phys. Res. B59/60 (1991) 491

[16] Deppe D. & N. Holonyak Jr., J. Appl. Phys. 64 (1988) R93

[17] Laidig W.D. et al, Appl. Phys. Lett. 38 (1981) 776

[18] Holonyak N. Jr. et al, Appl. Phys. Lett. 39 (1981) 776

[19] Klopfenstein P., G. Bastide J. Appl. Phys. 63 150 (1988)

[20] Meyerson B.S., IBM J. Res. Develop. 34, 806 (1990)

[21] Park J. S. et al, Appl. Phys. Lett. 64(18), 1994

[22] Lin T.L., Appl. Phys. Lett. 60 380 (1992)

[23] Tsaur B.Y., IEEE Electron Device Lett., 12 293 (1991)

[24] Cheung N.W. et al,Nucl. Instrum. Meth. Phys. Res. B37/38 (1989)

[25] Schrenkelkamp R.J. et al, Mater. Sci. Rep. 6 (1991) 1

[26] Williams J.S. et al, Mater. Res. Soc. Bull. 17(1992) 47

[27] Linnros J. et al, Phys. Rev. B 30, (1984) 3629

[28] Williams J.S. et al,Mater. Res. Soc. Symp. Proc. 37 (1985), 127

[29] Williams J. S. et al, Phys. Rev. Lett. 55 (1985) 1482

[30] Poate J.M. et al, Nucl. Instrum. Meth. Phys. Res. 55(1991) 533.

[31] Ridgway M.C., J. Appl. Phys. 71(1992) 1708

[32] Elliman R.G. et al, J. Appl. Phys. 71(1992) 1010

[33] Pearton S.J., Mater. Sci. Rep. (1990) 313

[34] Bryan R.P. et al, Appl. Phys. Lett. 55(1989) 94

[35] Lonnros J. et al, J. Mater. Res. 6 (1988) 1208

[36] Priolo F., E. Rimmi, Mater. Sci. Rep. 5 (1980) 319

[37] Vos M. et al, Appl. Phys. Lett. 58 (1991) 951

[38] Tsaur B.Y. et al, Nucl. Instrum. Meth 182/183 67 (1981)

[39] Raghavan V., in " Materials Science and Engineering"

[40] Hansen M., in "Constitution of Binary Alloys" (McGraw Hill 1958)

[41] Abeles B., T. Tiedje, Phys. Rev. Lett. 51, 2003 (1983)

[42] Prokes S.M., F. Spaepen, Appl. Phys. Lett. 47(3) 1985

[43] People R., J.C. Bean, Appl. Phys. Lett. 48(1986) 538

[44] Cris G Van De Walle, Phys. Rev. B 34(1986) 5621

[45] Soref R.A., F. Namver & J.P. Lorenzo, Optt. Lett 5 1990, 270

[46] Temkin H., T.P. Pearsall, J.C. Bean, R.A. Logan & A.S. Lurgi, Phys. Lett. 48(1986) 963

[47] Zachai R., K. Eberl, G. Absteiter, Phys. Rev. Lett. 64 (1990) 1055

[48] Matteson S et al, Nucl. Instrum. Meth. 182/183 (1981), 97

[49] Paine B.M. et al, Nucl. Instrum Meth. 182/183 (1981) 115

[50] Li J. et al, Nucl. Instrum. Meth. Phys. Res. B59/60 (1991) 989-993

[51] Zhu B. et al, Nucl. Instru. Meth. Phys. Res. B64 (1992) 108

[52] Chaudhari P., M.Tech Thesis, I.I.T. Kanpur (1993)

[53] Ramakrishnan K., M.Tech Thesis, I.I.T. Kanpur (1994)

[54] Banerjee N., Ph.D. Thesis I.I.T. Kanpur (1993)

[55] Homino Yuji et al, Pys. Lett. 105A, 4-5 (1984) 248-59

[56] Cheng Y.T. et al, Nucl. Instrum. Meth. Phys. Res. B59/60 (1991) 509-16

[60] Swanepoel R., J. Phys. E16 (1983) 1214-22

[61] Schroder D.K., in "Semiconductor Material and Device Characterization" A Wiley Interscience Publication.

[62] Averback R.S. ey al, J. Appl. Phys. 53(1982) 1342

[63] Desimoni J. et al, Nucl. Instrum. Meth. Phys. Res. B71 (1992) 22-25

[64] Lev R.Y. et al, Nucl.Instrum Meth. Phys. Res. B59/60 (1991) 532

[65] Martil I., and G.G. Diaz, Am. J. Phys., Vol 60 No.1 1992, 83-86

[66] Bube R.H. in Electronic properties of Crystalline Solids (Academic, New York 1974), Chapter 11.

[67] Cheng Y.T., Mater. Sci. Rep. 5 (1990) 45-97

[68] Corngold N.R., Phys. Rev. A 39(1989) 2126